이학석사 학위논문

Multi-omics research on the mechanism of the anti-tumor effect of nicotinamide supplement in triple-negative breast cancer

삼중음성유방암에 대한 니코틴아마이드의 항암 대사 기작에 관한 오믹스 연구

2022년 8월

서울대학교 대학원

생명과학부

임 예 빈

Multi-omics research on the mechanism of the anti-tumor effect of nicotinamide supplement in triple-negative breast cancer

지도교수 황 대 희

이 논문을 이학석사 학위논문으로 제출함
2022년 8월

서울대학교 대학원
생명과학부
임 예 빈

임예빈의 석사 학위논문을 인준함
2022년 7월

위 원 장 박 주 홍 (인)

부위원장 황 대 희 (인)

위 원 노 성 훈 (인)

Acknowledgements

This thesis has been published in the following article:

Jung, M., Lee, K.M., **Im, Y.**, Seok, S.H., Chung, H., Kim, D.Y., Han, D., Lee, C.H., Hwang, E.H., Park, S.Y., et al. (2022). Nicotinamide (niacin) supplement increases lipid metabolism and ROS-induced energy disruption in triple-negative breast cancer: potential for drug repositioning as an anti-tumor agent. Mol Oncol 16, 1795-1815.
Minsun Jung, Kyung-Min Lee, and Yebin Im contributed equally as the main authors.
Hyebin Lee, Daehee Hwang, and Han Suk Ryu jointly supervised this work.

Part of the experiments (section 2.1, 2.2, 2.4, 2.9–16) and result analyses (section 3.4) in this thesis were done by Jung, M., and Lee, K.-M., from Seoul National University Hospital.

Abstract

Triple-negative breast cancer (TNBC) is the most aggressive subtype of breast cancer with a poor prognosis. However, TNBC has been difficult to treat because it lacks specific target molecules. Therefore, a new therapeutic approach for TNBC is required. Nicotinamide (NAM) is a water-soluble amide derivative of niacin (vitamin B3) that plays an important role in mitochondrial metabolism and redox reactions. Previous studies have shown that NAM inhibits the growth and progression of various cancer cells, including TNBC. Here, we applied a multi-omics analytical approach to reveal the mechanistic link between NAM-induced metabolic regulation and the anti-tumor impact of NAM in TNBC. NAM decreased mitochondrial membrane potential and ATP production while increasing reverse electron transport (RET), fatty acid oxidation, and glycerophospholipid/sphingolipid metabolic pathways in TNBC, resulting in an increase in reactive oxygen species (ROS). The elevated levels of ROS initiated apoptosis and inhibited tumor development. Our findings revealed that NAM therapy causes cancer cell death in TNBC through mitochondrial malfunction and ROS activation via bifurcating metabolic pathways (RET and lipid metabolism). We propose that NAM supplement has a potential to be repositioned as a next-generation anti-metabolic agent for TNBC treatment, with the anticipation that our findings will pave the way for more advanced NAM use in clinical studies.

Keyword : triple-negative breast cancer, nicotinamide, functional genomics, cancer metabolism, reactive oxygen species
Student Number : 2020-21313

Table of Contents

Chapter 1. Introduction

1.1. Study Background

Triple-negative breast cancer (TNBC) is a molecular subtype of breast cancer defined by the absence or low expression of the estrogen receptor (ER), progesterone receptor (PR), and human epidermal growth factor receptor 2 (HER2) [1]. TNBC accounts for 15% to 20% of all invasive breast cancers, with the worst prognosis [2]. Unlike other breast cancer subtypes, TNBC is resistant to endocrine treatment and molecular targeted therapy because it lacks expression of ER, PR, and HER2 [3]. As a result of this restriction, nonspecific cytotoxic chemotherapy remains a primary treatment choice for TNBC. In addition, only one-third of patients are anticipated to have a therapeutic response, which motivates the development of innovative treatments [1,4].

The dysregulation and reprogramming of energy metabolism are one of the hallmarks of cancer that leads to uncontrolled tumor development and cell death resistance [5]. Therefore, therapies targeting altered metabolism have gained interest as a possible alternative to immunotherapy for the next generation of anti-tumor treatments [6]. Recently, metabolic medicines such as metformin and fluvastatin, which were once used to treat diabetes or dyslipidemia, have been effectively repositioned as anti-cancer adjuvants, with clinically favorable prognosis in breast cancer [7,8]. These findings provide credence to the possibility that additional non-cytotoxic yet effective alternatives for targeting malignant metabolism exist.

Nicotinamide (NAM) is a water-soluble amide derivative of

niacin (vitamin B3). It is readily absorbed by cells and functions as a precursor for the coenzyme NAM adenine dinucleotide (NAD+). The supplement's primary mechanism is to operate as an essential regulator of mitochondrial metabolism and redox processes [9]. NAM can be ingested via commonly available dietary supplements, such as vitamin B complex (NIAGEN, ChromDex Inc., Irvine, CA). In addition to its efficiency in preventing aging and preserving physiologic processes, NAM has lately attracted attention for its anti-tumor properties. By modulating SIRT 1/2-, p53-, AKT-, and PARP1-dependent cascades, NAM reduced the proliferation of several cancers including leukemia [10-13].

1.2. Purpose of Research

Previous research has demonstrated that nicotinamide inhibits TNBC cell viability in vitro [14]. In the current investigation, we integrated transcriptomics and proteomics to evaluate metabolic changes and biological responses produced by NAM at the global level in TNBC. The functional enrichment and network analysis of genes and proteins altered by NAM revealed a biological relationship between NAM-induced metabolic regulation and the apoptotic death of TNBC cells. In TNBC, NAM inhibited mitochondrial metabolism and elevated reactive oxygen species (ROS) via increasing the activity of the reverse electron transport (RET) pathway and lipid metabolism, resulting in apoptosis. As a consequence, we demonstrated convincing metabolic mechanism of NAM inhibiting tumor development in TNBC with computational methods. On the basis of these results, NAM could be a potential anti-cancer drug that targets the cancer metabolism in TNBC.

Chapter 2. Methods

2.1. Cell culture and chemicals

BT20 and MDA-MB-468 cell lines were obtained from the Korea Cell Line Bank (Seoul, Republic of Korea). MDA-MB-231 cells were purchased from the American Type Culture Collection (Manassas, VA, USA). BT20 cells were cultured in RPMI (Gibco, Carlsbad, CA, USA) containing 10% fetal bovine serum (FBS) (Invitrogen, Carlsbad, CA, USA) and 1% penicillin/streptomycin (PS) (Gibco). MDA-MB-468 and MDA-MB-231 cells were cultured in DMEM (Gibco) containing 10% FBS and 1% PS. Cells were maintained at 37 ° C in a humidified atmosphere of 95% air and 5% CO2 and periodically screened for mycoplasma contamination. All cell lines were confirmed by short tandem repeat DNA profiling tests. N-acetyl cysteine (NAC) and NAM were purchased from Sigma-Aldrich (St. Louis, MO, USA). A caspase inhibitor z-VAD.fmk was purchased from R&D Systems (Minneapolis, MN, USA).

2.2. RNA isolation, library preparation and sequencing

Total RNA was isolated from all cell lines (n = 3 per cell type) before and 48 h after treatment of 20 mm-NAM, using TRIzol® RNA Isolation Reagent (Invitrogen), and purified according to the manufacturer's instructions. The RNA concentration was determined using a NanoDrop ND-1000 spectrometer (Thermo Fisher, Waltham, MA, USA), and the RNA integrity number for each RNA sample was analyzed using a 2100 Bioanalyzer and the Agilent

RNA 6000 Nano Kit (Agilent, Santa Clara, CA, USA). The RNA integrity numbers (RINs) of all samples were higher than 8, which is appropriate for RNA sequencing. The isolated total RNA (1 μg) was utilized to generate cDNA libraries using the TruSeq RNA library kit (Illumina, San Diego, CA, USA), according to the manufacturer's instructions [14]. The libraries were quantified using qPCR based on the qPCR quantification protocol guide, followed by qualification using an Agilent 2100 Bioanalyzer (Agilent). The sequencing of each library was performed on an Illumina HiSeq 2500 platform and clusters of the cDNA libraries were generated on a TruSeq flow cell and sequenced for 76-bp paired end reads (2 × 76) with a TruSeq 200 cycle SBS kit (Illumina). Raw data were processed, and base calling was performed using the standard Illumina pipeline (CASAVA ver. 1.8.2 and RTA ver. 1.18.64, both provided by Illumina).

For the resulting peptide samples, tandem mass tag 6-plex labelling was performed according to the manufacturer's instructions, with modifications. After the labelled peptides were pooled, the sample was separated into 12 fractions using Agilent 1290 bioinert high-pH reverse-phase liquid chromatography (HPLC, Agilent) equipped with an analytical column (4.6 × 250 mm, 5 μm). HPLC was performed at a flow rate of 0.8 mL · min-1 on a 60-min gradient using Solvent A (15 mm ammonium hydroxide in water) and solvent B (15 mm ammonium hydroxide in 90% ACN). BT20 and MDA-MB-468 cell lines were obtained from the Korea Cell Line

2.3. Transcriptomic analysis

For the read sequences resulting from the RNA sequencing, the adapter sequences (TruSeq universal and indexed adapters) were

removed using the cutadapt software (ver. 2.8) [15]. The resulting reads were then aligned to the human reference genome (GRCh38) using tophat aligner (ver. 2.1.1) with the default options [16]. After the alignment, the mapped reads were counted for gene features (GTF file of GRCh38) using htseq (ver. 0.11.3) [17], and the fragments per kilobase of transcript per million mapped reads (FPKM) were estimated using the gene lengths in Ensembl (GRCh38 Release 99) using cufflinks (ver. 2.2.1) [18].

Next, we identified differentially expressed genes (DEGs) between NAM-treated samples and non-treated controls (NAM versus control) in each TNBC cell type using the previously reported statistical method [19]. Briefly, we first selected 'expressed' genes as the ones with FPKM values $\geq$ 1. The log2(FPKM+1) was then normalized using the quantile normalization method [20]. For each gene, we calculated the t-statistic values in the comparison of NAM versus control. We estimated an empirical null distribution of the t-statistic values and by performing random permutations of all samples 1000 times. Using the estimated empirical distribution, we computed the adjusted P-value for t-test for each gene. Finally, we identified DEGs as the ones that had t-test P-values < 0.05 and absolute log2-fold-changes > 0.58 (1.5-fold) cutoff.

2.4. Sample preparation and liquid chromatography-tandem mass spectrometry (LC-MS/MS)

Three TNBC cell lines (n = 3 per cell type) were lysed in SDS-lysis buffer. Following protein isolation, disulfide bonds were reduced, and sulfhydryl groups were alkylated with 50 mm Iodoacetamide (IAA) solution for 30 min at room temperature in the dark. After the

exchange of buffer with 50 mm triethylammonium bicarbonate (TEAB), the protein was digested at 37 ° C overnight using the filter-aided sample preparation procedure, as previously described [21], with a trypsin/LysC mixture at a 100 : 1 protein to protease ratio. LC-MS/MS analysis was conducted for each fraction of the peptide sample using a Q-exactive plus mass spectrometry (Thermo Fisher) coupled to an Ultimate 3000 RSLC system (Dionex) and a nanoelectrospray source, as previously described, with modifications [22]. The precursor ions were fragmented with high-energy collisional dissociation at a normalized collision energy of 32 with a resolution of 35 000 at m/z 200. The maximum ion injection times for the full scan and MS/MS scan were 20 and 100 ms, respectively. The detailed information for LC-MS/MS analysis can be found in previous studies [14,22]. Raw LC-MS/MS data were uploaded into PRIDE database (PXD005304).

2.5. Proteomic data processing and analysis

MS raw files were processed using proteome discoverer 2.1 software (Thermo Fisher). MS/MS spectra were searched with the Human UniProt database (December 2014, 88 657 entries) using the SEQUEST-HT search engine with forward and reverse protein sequences and common contaminants. Peptides matched to the MS/MS spectra with false discovery rates (FDRs) were determined using the Percolator software package. Reporter ion quantification was performed in the MS2 channel with a 20-ppm mass tolerance. Detailed search parameters can be found in a previous study [14]. Using the protein abundances, we next identified differentially expressed proteins (DEPs) between NAM-treated samples and

non-treated controls (NAM versus control) in each TNBC cell type by applying the aforementioned empirical t-test to the normalized protein abundances. After manual inspection of protein abundances between NAM and control, we initially selected DEPs as the proteins with adjusted P-values < 0.2 and absolute log2-fold-changes > 0.26, 0.28, and 0.33 for BT20, MDA-MB-468, and MDA-MB-231, respectively. The cut-off was determined as the mean of 2.5th and 97.5th percentiles of the empirical null distribution for log2-fold-changes for each TNBC cell type. To further remove false positives, the absolute gaps between NAM and control were calculated for the selected DEPs as the differences between the minimum and maximum abundances in the conditions with high and low mean abundances, respectively. Among the initially selected proteins, we finally selected the final DEPs as the ones with the absolute gap > 0.058, 0.06 and 0.077 for BT20, MDA-MB-468, and MDA-MB-231, respectively. The cutoff was determined as the mean of 25th and 75th percentiles of the gap distribution in each TNBC cell type.

2.6. Gene ontology annotation enrichment analysis

To identify the cellular processes represented by the list of genes or proteins, we performed the enrichment analysis of gene ontology biological processes (GOBPs) for the genes or proteins using DAVID software [23] and then selected the GOBPs with P-value < 0.05 from Expression Analysis Systematic Explorer (EASE) test. To examine the associations among the GOBPs represented by upregulated or downregulated genes/proteins, we next reconstructed a network model where the nodes and edges respectively denote the

GOBPs and the associations between the pairs of GOBPs. Two nodes were connected when (a) the number of shared genes (or proteins) commonly involved in the two corresponding GOBPs was ≥3 and (b) the Sørensen-Dice coefficient was > 0.56 for upregulated GOBPs and > 0.32 for downregulated GOBPs. Here, the Sørensen-Dice coefficient between nodes i and j was determined as $2|Pi \cap Pj|/(|Pi| + |Pj|)$, where |Pi| and |Pj| are the numbers of genes/proteins involved in the GOBPs corresponding to nodes i and j, and $|Pi \cap Pj|$ is the number of the shared genes/proteins mentioned above, as previously described [24,25]. We determined the cut-off (0.56 and 0.32) at the 95th percentile in the coefficient distribution, which was estimated using the coefficients for all possible pairs of nodes with $|Pi \cap Pj| \geq 3$ in the network of upregulated or downregulated GOBPs. For visualization in Cytoscape ver. 3.8.2 [26], we used the Community Clustering (GLay) algorithm to the nodes using the CLUSTERMAKER2 plugin [27], and the resultant node clusters were further grouped into four modules (metabolism, cell proliferation, cell development and immune response).

2.7. Reconstruction of molecular network models for DEGs and DEPs

To reconstruct molecular network models, we selected DEGs/DEPs involved in the selected GOBPs. The interactions among the DEGs/DEPs were obtained from metabolic reactions in KEGG pathway database [28-30]. The resulting networks were visualized using Cytoscape, and the nodes were arranged according to the information in the related KEGG pathways.

2.8. Analysis of mRNA-seq data from TCGA breast cancer cohort

The mRNA-seq dataset for human breast cancer tissues (TCGA-BRCA) was obtained from TCGA genomic data commons (GDC) data portal [31] together with clinical information. Among all the samples in the TCGA-BRCA dataset, we selected 650 breast cancer samples belonging to luminal A, luminal B and TNBC histological subtypes. Note that the HER2-positive samples were excluded due to the small sample size (29 samples). We downloaded FPKM values of 60 483 genes for 650 samples and then selected the genes with FPKM > 1 in more than 50% of the tumor samples as expressed genes in each subtype. After converting the FPKM values to $\log_2$(FPKM + 1), they were normalized using the aforementioned quantile normalization method. We then applied the empirical t-test mentioned above to the normalized data for the comparison of TNBC (115 samples) versus non-TNBC (luminal A and luminal B, 535 samples). Finally, we identified DEGs as the ones that had t-test P-values < 0.05 and absolute log2-fold-changes > 0.18 cut-off (the mean of 2.5th and 97.5th percentiles of the empirical null distribution).

2.9. Measurement of mitochondrial membrane potential

Mitochondrial membrane potential ($\Delta\psi$m) was analyzed by cationic dye 5,5′,6,6′-tetrachloro-1,1′,3,3′-tetraethylbenzimi-dazolylcarbocyanine iodide (JC-1, Invitrogen) and MitoTracker Red (CMXRos; Molecular Probes, Carlsbad, CA, USA) staining. Briefly, NAM treated cells were incubated with JC-1

for 20 min followed by two washes using PBS prior to emission measurements. The emission was measured at 590 and 540 nm after excitation at 480 nm using a multimode microplate reader (Glomax® Explorer; Promega, Madison, WI, USA). For MitoTracker Red analysis, cells were stained with MitoTracker Red (5 μm) for 30 min at 37 ° C and analyzed by flow cytometry and processed using the FLOWJO™ 10 software (BD Biosciences, San Diego, CA, USA). Fluorescent images of the cells were taken under a fluorescent microscope (Leica, Zeiss, Germany).

2.10. Oxygen consumption rate (OCR) and real-time ATP rate analysis

The Mito Stress Test Kit (Cat. 103015-100; Agilent) was used to measure the OCR. The Seahorse XF Real-Time ATP Rate Assay Kit (Cat. 103592-100; Agilent) was used to detect the ATP production rates of mitochondrial oxidative phosphorylation (OXPHOS). Cells were seeded into XF-24 cell culture microplates (Seahorse Bioscience, North Billerica, MA, USA) at a density of 40 000-60 000 cells per well and allowed to adhere on a plate overnight. After incubating the cells with NAM for 24 h, OCR and real-time ATP production rates of mitochondrial OXPHOS were determined and analyzed on the Seahorse Bioscience XF-24 Extracellular Flux Analyzer (Agilent) according to the manufacturer's instructions. For the measurement of OCR value, oligomycin, fluoro-carbonyl cyanide phenylhydrazone (FCCP), and Rotenone/Antimycin A (Rot/AA) were added in order according to the manufacturer's protocols. For the determination of ATP production rates of mitochondrial OXPHOS and glycolysis, oligomycin

and a mix of Rot/AA was added.

2.11. Measurement of NAD+/NADH ratio

NAD+ and NADH levels were measured using a NAD+ /NADH quantitation kit (Sigma-Aldrich). Briefly, 5 9 105 cells were lysed. The NAD+ level was measured by subtracting the NADH concentration from the total NAD concentration. Data were normalized to total protein content determined by using the BCA protein assay.

2.12. Quantification of Intracellular ROS

For 2' -7' dichlorofluorescin diacetate (DCFH-DA; Sigma-Aldrich) assay, cells were cultured under standard culture conditions up to 80% confluency and different concentrations of NAM was added for 1 h in stressed labelled cells and then incubated at 37 ° C with 5 μM DCFH-DA for 15 min. The fluorescence intensity was measured at 485-excitation and 530-emission by fluorimeter as fluorescence units. It was normalized relative to the control as an oxidative stress index. For intracellular hydrogen peroxide (H2O2) assay, cells were treated with NAM for 24 h in white-walled clear bottom 96-wells plate and intracellular ROS levels were analyzed by ROS-GloTM H2O2 assay kit (Promega) following the manufacturer' s guidelines. Luminescence was measured using a luminometer (Glomax Explore Multimode Microplate Reader).

2.13. Cell viability assay

The procedures described in a previous study were followed [32]. Cells were plated in triplicate (3000 cells per well) and incubated in a medium containing 10% FBS. After 24 h, the complete medium was replaced with the test medium containing the vehicle control and various doses of NAM for 48 h at 37℃. Cell viability was assessed by measuring the intracellular levels of ATP using the Cell Titer-Glo luminescent cell viability assay kit (Promega). Luminescence was measured using a luminometer (Glomax Explore Multimode Microplate Reader). To investigate cytotoxicity effects of N-acetyl cysteine (NAC) or z-VAD.fmk, cells were seeded into white-walled 96-well microplates and treated with NAC or z-VAD.fmk for 1 h prior to NAM treatment. Following the treatment, an equal volume of Caspase-Glo 3/7 reagent was added and the luminescence signal was detected using the Glomax-Multi Detection System (Promega).

2.14. Flow cytometry analysis

The procedures described in a previous study were followed [32]. Cell apoptosis assay was performed using the annexin V-FITC/propidium iodide (PI) apoptosis detection kit (BD Biosciences). Briefly, cells were collected, washed twice with PBS, and then suspended in 300 μL of binding buffer. Annexin V solution (5 μL) was added to the cell suspension and incubated for 15 min in the dark at room temperature. Subsequently, 200 μL of binding buffer and 5 μL of PI were added, and the cell suspension was immediately analyzed on a BD FACSCaliber (BD Biosciences). All data were processed using the FLOWJO™ 10 software.

2.15. Quantitative real-time polymerase chain reaction (qPCR) and qPCR array

Total RNA was isolated from cells using the AccuPrep Universal RNA Extraction Kit (Bioneer, Daejeon, Korea) after 24 h of NAM treatment according to the manufacturer's protocol. Genomic DNA was removed by DNase treatment using RNase-Free-DNase Set (Qiagen, Hilden, Germany). cDNA was synthesized using AccuPower RocketScript Cycle RT PreMix (Bioneer). All data were analyzed based on the relative quantification, with normalization to glyceraldehyde 3- phosphate dehydrogenase (GAPDH) expression for the assessment of ACSL3, CPT2, CPT1A, HADHB and ETFDH genes and to the reference gene RPL13A for solute carrier (SLC) array. The DDCT value was used to determine the relative fold change.

2.16. Western blotting

Cells were collected and homogenized using radioimmunoprecipitation assay (RIPA) lysis buffer (Thermo Fisher) on ice. Subsequently, the cell lysates were centrifuged at 4℃ to isolate the proteins. Proteins were quantified using the bicinchoninic acid protein assay kit (Thermo Fisher). Western blotting was performed using anti-c-caspase 3 (CST, Danvers, MA, USA), anti-PARP antibody (CST) and OXPHOS cocktail, including NDUFBB, SDHB, MTCO1, UQCRC2 and ATP5A (Abcam, Cambridge, UK). Anti-GAPDH antibody (BD Biosciences) or anti-HSC70 antibody (Thermo Fisher) was used as the loading control and quantification

of blotting bands were assessed by densitometry (IMAGEJ LAB software, National Institutes of Health, Bethesda, MD, USA).

Chapter 3. Results

3.1. Transcriptomic analysis showed that NAM inhibits mitochondrial activity by RET-mediated ROS generation

To determine how NAM regulates metabolism in TNBC cells, we applied mRNA-seq analysis that systematically investigates the molecular pathways controlled by NAM (Fig. 1A). In the mRNA-seq data, we identified a total of 1,983 upregulated and 2,035 downregulated genes in NAM-treated cells, relative to non-treated controls, in the three cell types: 2,194 DEGs (987 upregulated and 1,107 downregulated) in BT20, 1,480 DEGs (641 upregulated and 839 downregulated) in MDA-MB-468, and 1,232 DEGs (737 upregulated and 495 downregulated) in MDA-MB-231 (Fig. 1B). Among DEGs, only 40 upregulated and 34 downregulated genes (0.020% and 0.0170% of total 1,983 upregulated and 2,035 downregulated genes, respectively) overlapped in all TNBC cell types, whereas the majority of DEGs exhibited cell-type-specific differential expression (Fig. 1C, D and Table 1).

Despite the minimal overlap of DEGs at the molecular level, we then evaluated whether the cellular processes represented by DEGs in the distinct cell types were shared by all three kinds of TNBC cells. We selected GOBP terms that were enriched by DEGs in each cell type and investigated whether the enriched GOBP terms were shared by the three kinds of TNBC cells. The majority of the upregulated genes in the individual cell types were associated with cell death processes (programmed cell death, autophagy, and apoptotic mitochondrial changes) and mitochondrial processes (organization,

pH reduction, oxidation-reduction, response to starvation, respiratory chain assembly, and NADP/lipid/oxoacid metabolism (Fig. 1E, 'Up' panel). Intriguingly, lipid metabolism and amino acid transport/metabolism (glutamine metabolic pathway) were also increased in one or two subtypes of TNBC cells. Among them, cellular responses to starvation and programmed cell death were consistently upregulated in all the three TNBC cell types, confirming the previously suggested NAM-induced apoptosis [14]. On the other hand, the processes related to immune response (NF-kB and mitogen-activated protein kinase signaling, cell adhesion/migration, and response to cytokine) and cell proliferation were downregulated consistently in all the three TNBC cell types (Fig. 1E, 'Down' panel).

We next examined whether the cellular processes represented by DEGs in the distinct cell types were shared by all three kinds of TNBC cells, although low overlapping of DEGs was shown at the molecular level. We identified GOBPs enriched by the DEGs in each cell type and examined whether the enriched GOBPs were shared among the three types of TNBC cells. The upregulated genes in the individual cell types were mainly associated with the processes related to cell death (programmed cell death, autophagy and apoptotic mitochondrial changes) and mitochondria (organization, pH reduction/redox/NADP metabolism, response to starvation, respiratory chain and lipid/ oxoacid metabolism) (Fig. 1E, 'Up' panel). Interestingly, lipid metabolism and amino acid transport/metabolism (glutamate metabolic process) were also upregulated in one or two TNBC cell types. Among them, cellular responses to starvation and cell death were consistently upregulated in all the three TNBC cell types, reiterating NAM-induced apoptosis

as previously reported [14]. On the other hand, the processes related to immune response (NF-κB and mitogen-activated protein kinase signaling, cell adhesion/migration, and response to cytokine) and cell proliferation were downregulated consistently in all the three TNBC cell types (Fig. 1E, 'Down' panel). To investigate how the mitochondrial processes affected by NAM are collectively linked to mitochondrial dysfunction, we built a network model describing the interactions among the DEGs involved in the aforementioned mitochondria-related processes (NADP metabolism, lipid modification, mitochondrion organization, and respiratory chain complex) from the three cell types of TNBC. The network model suggested that NAM was converted to NAD+ by NAMPT and NMNAT1 and then transported to the mitochondria via SLC25A51 transporter (Fig. 1F) [33]. To verify this result, we measured NAD+/NADH ratios in NAM-treated and non-treated TNBC cells; NAD+/NADH ratios were consistently higher in all the three types of NAM-treated TNBC cells (BT20, P = 0.0002; MDAMB-468, P = 0.001; MDA-MB-231, P = 0.0003) (Fig. 1G). In addition, the network model showed ETFDH upregulation and the increased levels of enzymes (NDUFA2/A4L2/A6/A7/B2/B6) of OXPHOS complex I (CI), suggesting that the RET pathway was triggered to revert NAD+ to NADH (Fig. 1H) [34]. Using qPCR, we verified that the upregulation genes involved in fatty acid b-oxidation, ACLS3 (BT20, P = 0.0004; MDA-MB-468, P = 0.0009; MDA-MB231, P = 0.0007), CPT2 (BT20, P = 0.0003; MDA-MB468, P = 0.0005; MDA-MB-231, P = 0.0008), CPT1A (BT20, P = 0.0042; MDA-MB-468, P = 0.0049; MDAMB-231, P = 0.0031), HADHB (BT20, P = 0.0004; MDA-MB-468, P = 0.0008; MDA-MB-231, P = 0.0009), and ETFDH (BT20, P = 0.0304; MDA-MB-468, P = 0.0029; MDA-MB-231, P

= 0.029), after NAM treatment (Fig. S1). Fatty acid b-oxidation facilitates over-reduction of coenzyme Q, which in turn promotes more RET [35]. Moreover, the levels of enzymes (IDH2 and SUCLG2) involved in the TCA cycle decreased in connection with the electron flux towards RET (Fig. 1F). As the reduction of NAD+ to NADH in OXPHOS CI during RET generates high levels of ROS [34], these findings suggested that RET-ROS generation might be involved in NAM-induced mitochondrial damage in TNBC cells.

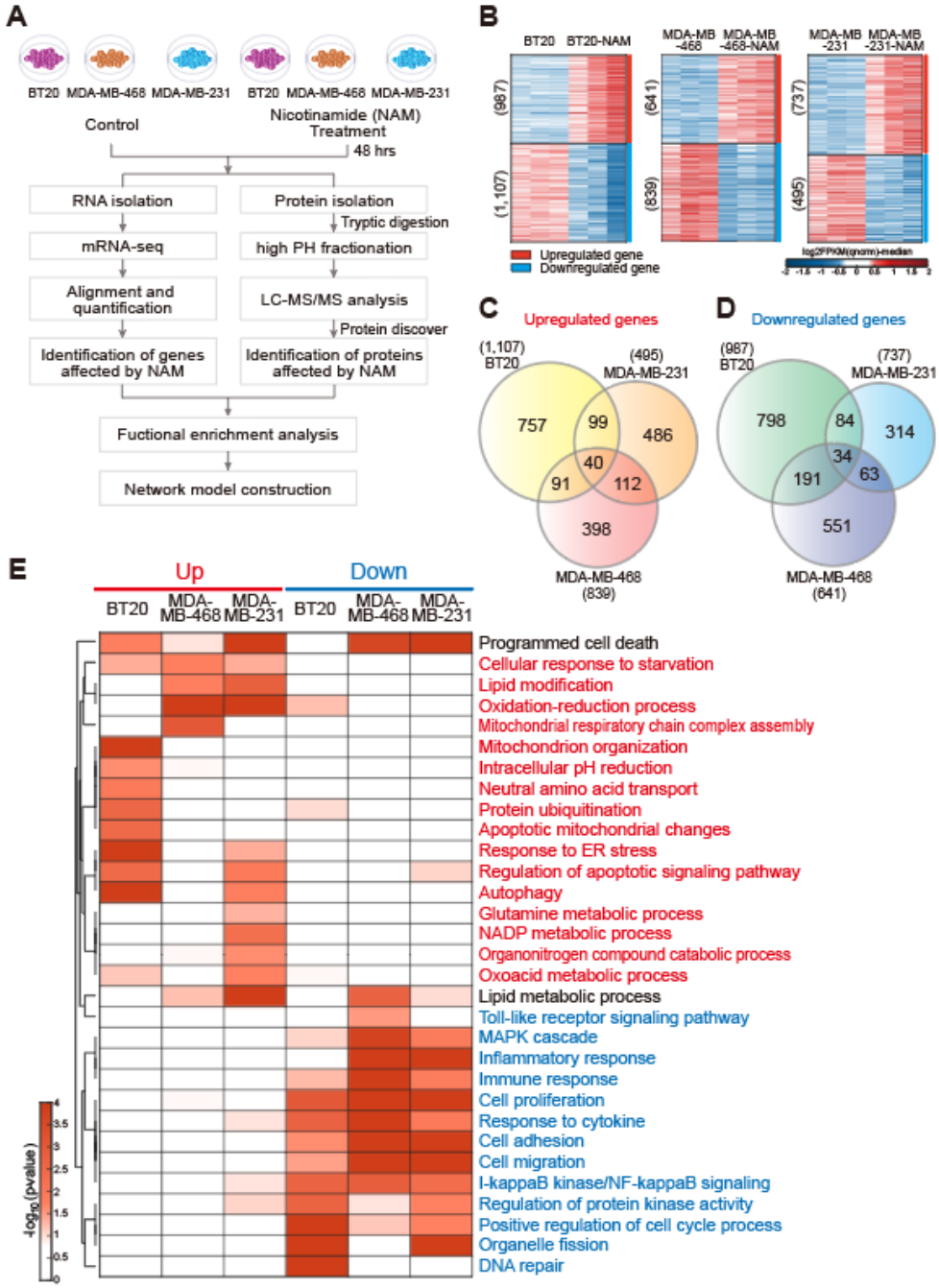
A
BT20 MDA-MB-468 MDA-MB-231 BT20 MDA-MB-468 MDA-MB-231
Control
Nicotinamide (NAM) Treatment
48 hrs
RNA isolation
Protein isolation
Tryptic digestion
mRNA-seq
high PH fractionation
Alignment and quantification
LC-MS/MS analysis
Protein discover
Identification of genes affected by NAM
Identification of proteins affected by NAM
Fuctional enrichment analysis
Network model construction
B
BT20 BT20-NAM
MDA-MB -468 MDA-MB -468-NAM
MDA-MB -231 MDA-MB -231-NAM
(987)
(1,107)
(641)
(839)
(737)
(495)
Upregulated gene
Downregulated gene
C
Upregulated genes
(1,107) BT20
(495) MDA-MB-231
757
99
486
40
91
112
398
MDA-MB-468 (839)
D
Downregulated genes
(987) BT20
(737) MDA-MB-231
798
84
314
34
191
63
551
MDA-MB-468 (641)
E
Up
Down
BT20
MDA-MB-468
MDA-MB-231
BT20
MDA-MB-468
MDA-MB-231
Programmed cell death
Cellular response to starvation
Lipid modification
Oxidation-reduction process
Mitochondrial respiratory chain complex assembly
Mitochondrion organization
Intracellular pH reduction
Neutral amino acid transport
Protein ubiquitination
Apoptotic mitochondrial changes
Response to ER stress
Regulation of apoptotic signaling pathway
Autophagy
Glutamine metabolic process
NADP metabolic process
Organonitrogen compound catabolic process
Oxoacid metabolic process
Lipid metabolic process
Toll-like receptor signaling pathway
MAPK cascade
Inflammatory response
Immune response
Cell proliferation
Response to cytokine
Cell adhesion
Cell migration
I-kappaB kinase/NF-kappaB signaling
Regulation of protein kinase activity
Positive regulation of cell cycle process
Organelle fission
DNA repair
-log10(pvalue)

(Continued)

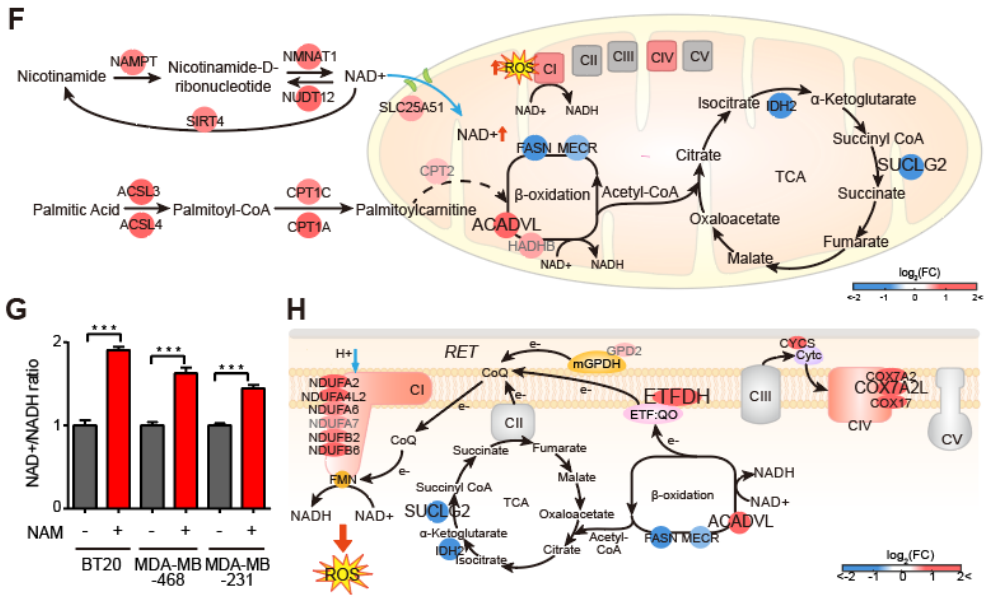

Figure 1. mRNA signatures associated with NAM-induced mitochondrial dysfunctions. (A) Overall scheme for mRNA-seq (left) and LC-MS/MS (right) analyses. (B) Heat maps showing log2-fold-changes of up- (red) and downregulated (blue) genes in BT20 (left), MDA-MB-468 (middle) and MDA-MB-231 (right) triple-negative breast cancer (TNBC) cells (color bar, gradient of $\log_2$(fold-changes) of DEGs; numbers of up- or downregulated genes are in parenthesis). (C, D) Venn diagrams showing relationships among up- (C) and downregulated (D) genes in the three TNBC cells (total = 1983 and 2035, respectively). (E) Heat map showing the significance of cellular processes (gene ontology biological processes) being enriched by up- (left, red) and downregulated (right, blue) genes in the indicated cell types (color bar, gradient of -log10(P); P = enrichment P-value from EASE test). (F) Network model describing metabolic reactions altered by nicotinamide (NAM) treatment and the enzymes. Arrows indicate directions of the reactions, light blue arrows denote transport of indicated molecules, and dotted arrows

indicate indirect reactions involving intermediate reactions between the nodes. Node or OXPHOS complex colors represent up- (red) and downregulation (blue) of the corresponding gene or complex (color bar, gradient of log2-fold-changes, NAM versus control). The maximum log2-fold-changes in the three cell types were chosen for the node color. Node label size denotes whether the corresponding gene was identified as a DEG in three (large), two (middle) or one (small) of the cell types. Grey node labels denote that the corresponding nodes are non-DEGs in the three cell types. (G) NAD+ /NADH ratio in the three TNBC cell types after 10 mM of NAM treatment for 24 h (mean ± SEM from triplicate experiment. Comparisons were made using a two-tailed t-test, ***P < 0.001). (H) Network model describing RET-related metabolic reactions affected by NAM treatment. See the legend in (F) for the nodes and edges. (Abbreviations: CI to V, OXPHOS complexes I to V; CoQ, coenzyme Q; Cytc, cytochrome c; e-, electron; ETF:QO, electron-transferring flavoprotein dehydrogenase; FMN, flavin mononucleotide; mGPDH, mitochondrial glycerol 3-phosphate dehydrogenase; NAD(H), nicotinamide adenine dinucleotide; RET, reverse electron transport; ROS, reactive oxygen species; TCA, tricarboxylic acid cycle).

Table 1. Commonly up- and downregulated genes from all three TNBC cell lines

Upregulated genes (n=40)		Downregulated genes (n=34)	
GABARAPL2	CFAP36	JADE2	ALDH1A3
ERO1B	LARP6	TCOF1	ZBED6CL
TMEM14A	ETFDH	TRIP13	S100A2
PIGH	RAB33B	TRIP6	VARS
PLD3	CFAP53	CCDC80	UCA1
RNF141	HIST1H2AC	ZMYND8	MEX3A
ENO2	TTC32	MSLN	IKBKE
SAYSD1	PGBD2	ARHGDIB	LINC01764
SLC1A4	C6orf1	GBP1	
SIPA1L2	HHLA3	PSPC1	
STX12	LOC100506100	SPDEF	
CLU	TMEM191A	C3	
CSTA	MIR4712	TNS3	
TMX4	LINC01842	ALDH1B1	
CHAC1		SORD	
RSPH3		HDGF	
ACSS2		PLEKHS1	
STXBP1		SERPINH1	
RRNAD1		JPH2	
C7orf26		CTSS	
B3GAT3		RBPMS2	
IL18		STAT6	
SLC25A4		ELFN2	
SLC13A3		MLKL	
HIST1H2BD		FJX1	
ATF3		FZD2	

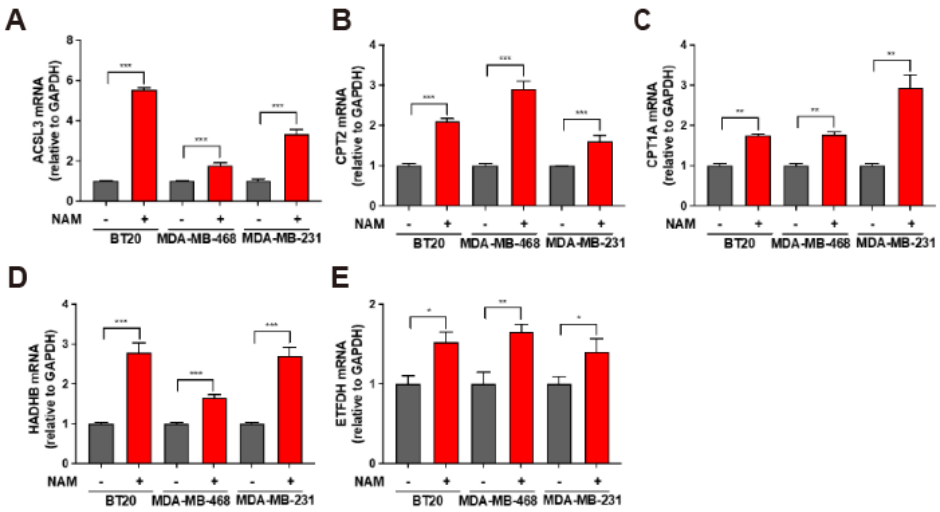

Figure S1. The expression levels of genes involved in fatty acid β-oxidation. NAM-induced changes (20mM, 24 hours) in expression of ACSL3 (A), CPT2 (B), CPT1A (C), HADHB (D), and ETFDH (E) genes by real-time PCR in all three TNBC cell types (two-tailed t-test $*p < 0.05$, $**p < 0.01$, $***p < 0.001$ from triplicate experiments).

3.2. Proteogenomic analysis identified NAM induced alteration of lipid metabolism and apoptosis

NAM-induced modulation linked to mitochondrial dysfunction may involve transcriptional and posttranscriptional changes that can be observed at the protein level. To augment protein signatures associated with the effect of NAM, we performed proteomic profiling of all the TNBC cell lines (BT20, MDA-MB-468 and MDA-MB-231). After protein isolation, tryptic digestion and TMT labelling, each labelled peptide sample was fractionated into 12 fractions by employing the previously reported high-pH fractionation method [22], and the individual fractions were then analyzed using LC-MS/MS (Fig. 1A). From the LC-MS/MS data, peptides were identified using the SEQUEST-HT search engine with an FDR of 1%, corresponding to 9,437 proteins, and the abundance of these proteins was estimated using PROTEOME DISCOVERER 2.1 (Thermo Fisher Waltham, MA, USA).

We identified the total number of 535 upregulated and 659 downregulated proteins in NAM-treated cells, compared to non-treated controls in the three cell types: 490 DEPs (182 upregulated and 308 downregulated) in BT20, 463 DEPs (210 upregulated and 253 downregulated) in MDA-MB-468 and 485 DEPs (232 upregulated and 253 downregulated) in MDA-MB-231. Similar to the DEGs, only a small fraction of the upregulated (8 of 535, 1.50%) and downregulated proteins (32 of 659, 4.86%) were shared across the three TNBC cell lines (Fig. 2A, B, Table 2). Moreover, among the total DEPs, 216 (40.4% of 535) upregulated proteins and 280 (42.5% of 659) downregulated proteins overlapped with the aforementioned 1,983 upregulated and 2,035 downregulated DEGs in Fig. 2C, D,

respectively, indicating that they were regulated consistently at both the mRNA and protein levels after NAM treatment (Fig. 2C, D). We then investigated whether cellular processes were commonly represented by the DEPs and DEGs. We first performed GOBP enrichment analysis independently for the following four molecular sets: (1-2) upregulated or downregulated genes and (3-4) upregulated or downregulated proteins. For effective comparison of GOBPs, we examined those level 1 GOBPs that were predominantly enriched by the four molecular sets; we found that the top GOBPs included metabolism, cell development, cell proliferation and immune response for both DEGs and DEPs (Fig. 2E). We therefore categorized level 2-4 GOBPs enriched by the four molecular sets into the level 1 GOBPs and integrated the categorized GOBPs into a GOBP association network, wherein nodes were enriched GOBPs and two nodes were connected when the molecules involved in the corresponding GOBPs were highly overlapping. The GOBP association network for upregulated genes and proteins showed that the processes related to cell death (apoptotic signaling and response to ER stress) and metabolism (mitochondrial organization, redox, cellular respiration/respiratory chain, glycerophospholipid/ sphingolipid metabolism and glutamate metabolism) were consistently enriched by both upregulated genes and proteins (Fig. 2F, S2). On the other hand, the GOBP association network for downregulated genes and proteins showed that the processes related to cell development (epithelial cell differentiation and angiogenesis), immune response (cell adhesion/migration, and cytokine production/response to cytokine) and cell cycle (DNA repair and cell division/cycle) were consistently enriched by both downregulated genes and proteins (Fig. 2G, S2).

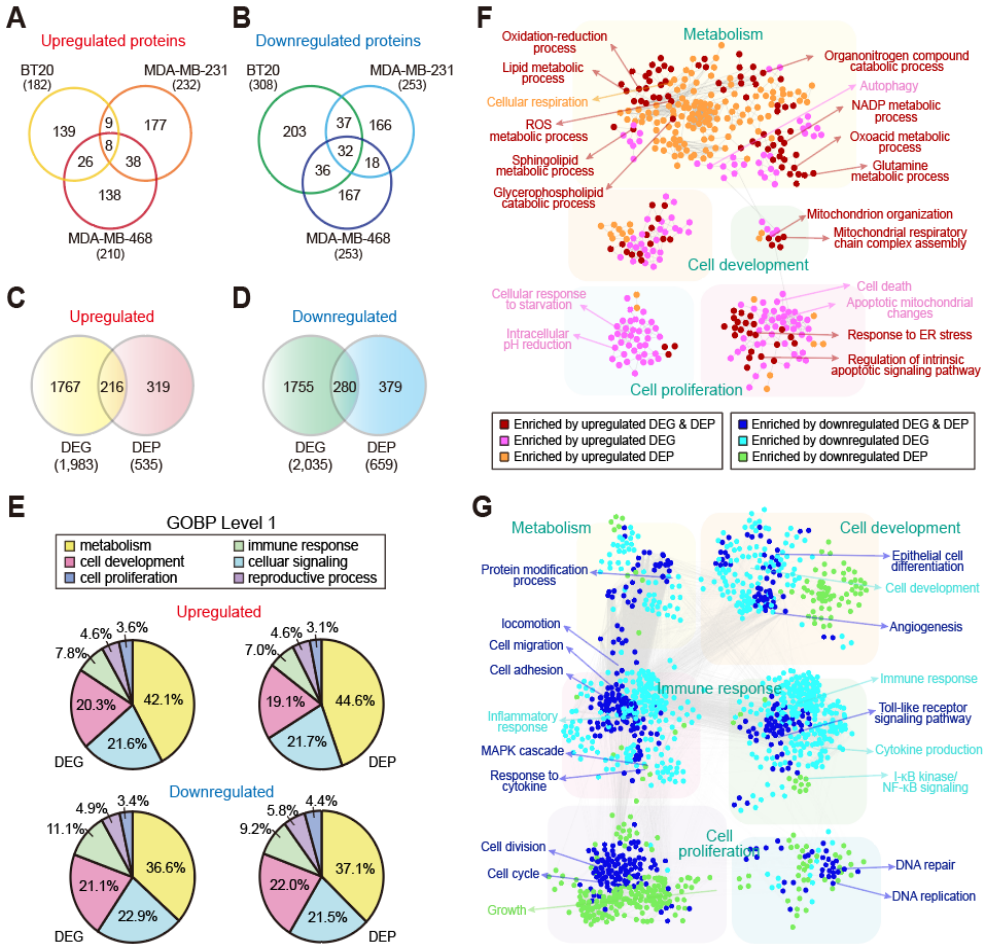

Figure 2 Protein signatures associated with NAM-induced mitochondrial dysfunctions. (A, B) Venn diagrams showing relationships among upregulated and downregulated proteins in the three triple-negative breast cancer (TNBC) cells (total = 535 and 659, respectively). (C, D) Relationships between the total up- and downregulated genes and proteins. (E) Pie charts showing the percentage of upregulated (top) and downregulated (bottom) genes (left) or proteins (right) involved in the indicated level 1 gene ontology biological processes (GOBPs). (F) GOBP association networks for GOBPs enriched by upregulated genes and/or proteins. (G) GOBP association networks for GOBPs enriched by

downregulated genes and/or proteins. GOBP nodes were arranged into four modules (metabolism, cell proliferation and development, and immune response). Edges between GOBP nodes indicate a significant overlap between genes or proteins involved in the corresponding GOBPs.

Table 2. Up/downregulated proteins from all three TNBC cell lines

Upregulated proteins (n=8)		Downregulated proteins (n=32)	
GLS		CCNA2	PRC1
SLC25A4		CCNB1	CCNB2
CNNM4		CDC20	ESPL1
H1-10		CNN2	KIF20A
H1-0		GLUL	UBE2E3
GXYLT1		BTF3	KIF2C
CCDC175		KPNA2	UBE2C
HSD17B7		MKI67	SPATS2L
		TPX2	UBE2T
		ECT2	NUSAP1
		PLK1	MIS18A
		RRM1	RAD18
		RRM2	TNS3
		AURKA	QSER1
		TTK	
		TYMS	
		DLGAP5	
		CNBP	

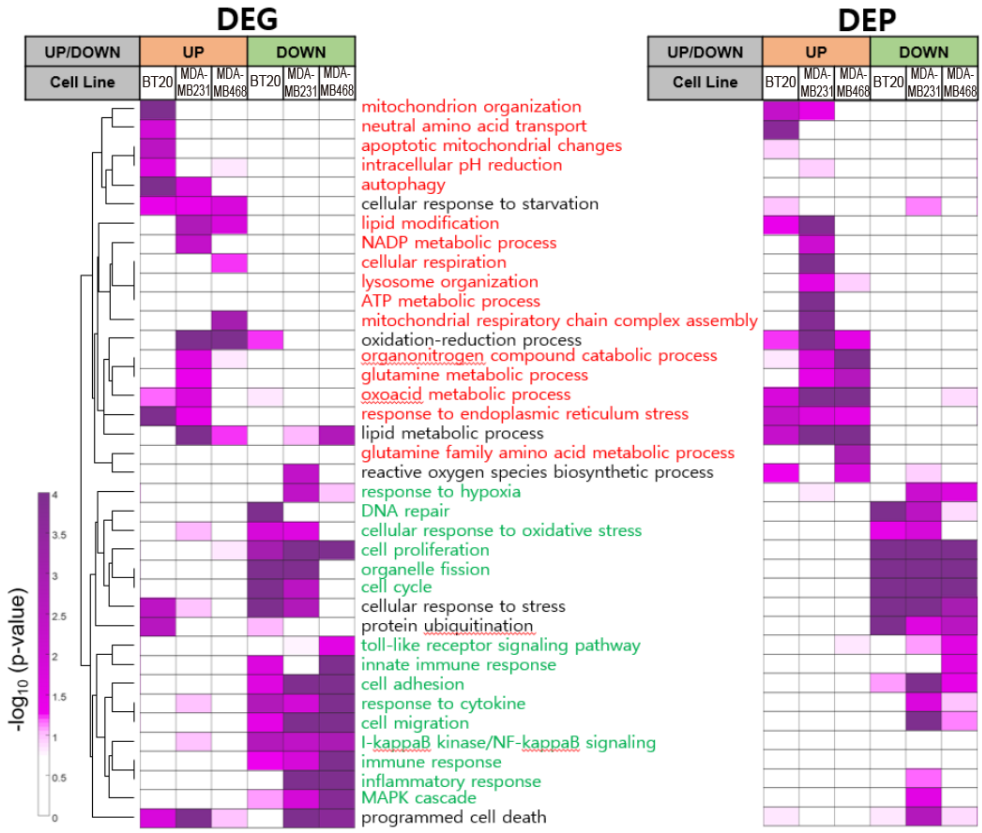

Figure S2. Heat maps of GOBPs enriched by DEGs and DEPs show consistency. GOBPs enriched by upregulated and downregulated genes are shown left. GOBPs enriched by upregulated and downregulated proteins are shown right. GOBP terms enriched by up regulated genes and proteins are colored in red. GOBP terms enriched by downregulated genes and proteins are colored in green.

3.3. NAM-induced metabolic alterations in proteogenomic networks converged on ROS generation and ROS-mediated apoptosis in TNBC

In addition to the NAM-induced RET pathway and fatty acid β-oxidation, the cellular processes enriched by the upregulated genes and proteins included glycerophospholipid/sphingolipid and glutamate metabolism. Several studies have reported that NAM maintains de novo lipogenesis [36] and glycerophospholipid /sphingolipid metabolic processes, which are linked to RET and apoptosis [37-39]. To determine the cumulative effects of these metabolic processes on NAM-induced mitochondrial dysfunction and cellular apoptosis, we extended the mRNA network model and include glycerophospholipid/sphingolipid and glutamate metabolic pathways based on both mRNA and protein data (Fig. 3). The extended network model showed that NAM increased the mRNA and/or protein levels of the enzymes in the glycerophospholipid metabolic pathway to increase the level of glycerol-3-phosphate (G3P). Together with the upregulated ETFDH, the increased G3P can further enhance the RET pathway and generate RET-ROS (Fig. 3, bottom right). Moreover, NAM increased the mRNA and/or protein levels of the enzymes involved in sphingolipid metabolism by increasing the amount of ceramide, which can enhance apoptosis and ROS-mediated cell death (Fig. 3, bottom left). In addition to fatty acid b-oxidation, these data showed additional lipid metabolic pathways modulated by NAM, which eventually results in mitochondrial dysfunction and apoptosis. To examine clinical relevance of these findings, we next analyzed TCGA mRNA profiles of tumor tissues from 650 patients (115 TNBC, 373 luminal A and 162 luminal B) with BRCA. We first

examined key nodes in the above major processes associated with the activation of ROS (RET and glycerophospholipid/sphingolipid metabolism in Fig. 3) between TNBC and non-TNBC (luminal A and B). Note that 29 HER2- positive patients were excluded from the analysis due to its small sample size. Among the 58 key nodes with mRNA expression levels available in TCGA data, 14 were upregulated in TNBC than in non-TNBC, whereas 21 were downregulated (Fig. S3A-C). When these upregulated and downregulated genes were mapped into the above network model (Fig. 3), most of the key pathways (ETFDH and GPD2 in RET; CPT2 and HADHB in fatty acid b-oxidation; ACSL3, SPTLC1, PLPP1, and CPT1A in sphingolipid metabolism; and GDPD1 and DGKQ in glycerophospholipid metabolism) were found to be downregulated in TNBC, as well as apoptosis-related genes (BIM and PUMA) (Fig. S3D). These data suggest that the activities of the key apoptosis-inducing processes upregulated by NAM are generally decreased in TNBC, supporting a potential therapeutic value of NAM in patients with TNBC.

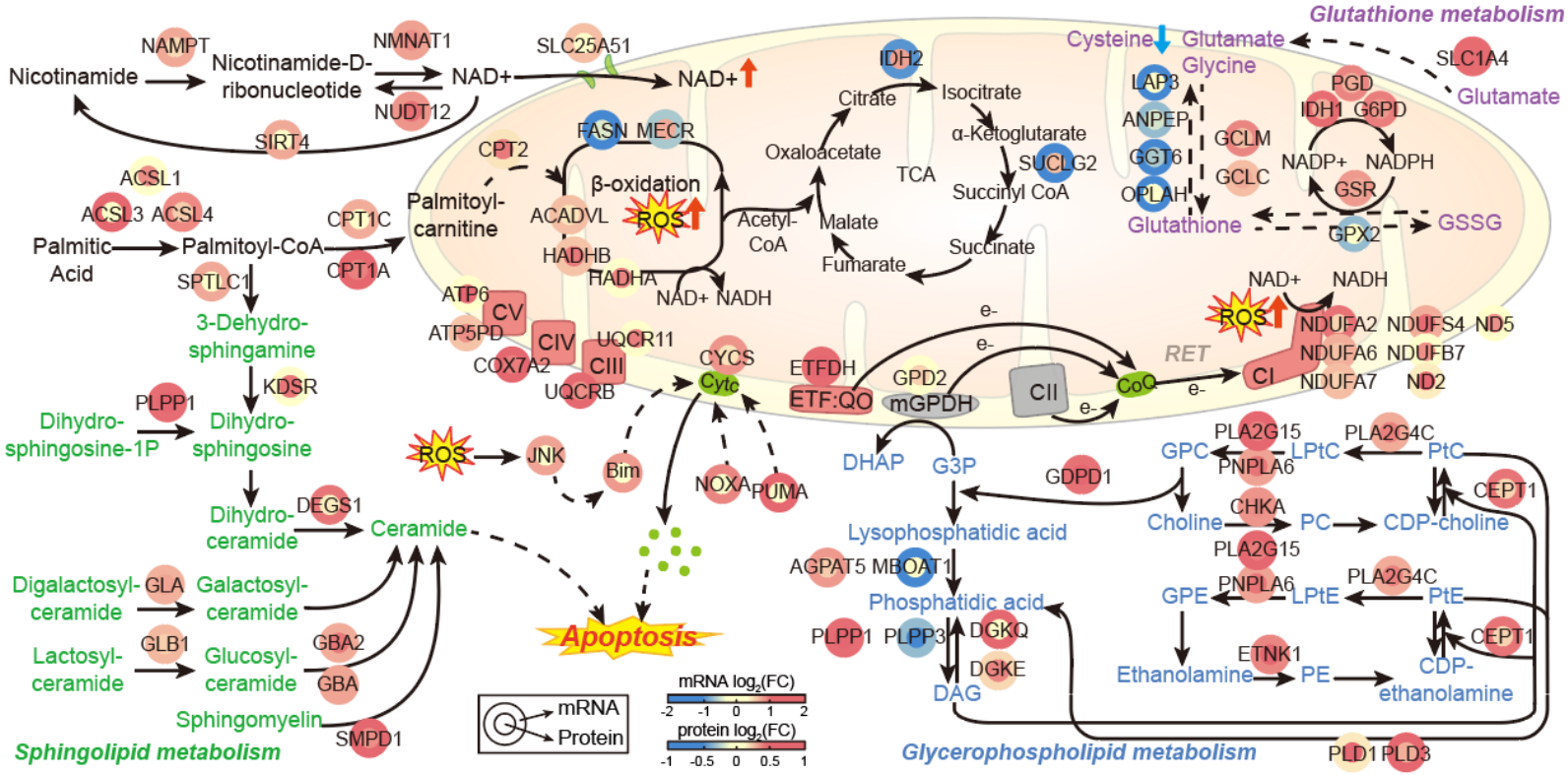
Glutathione metabolism
Cysteine
Glutamate
Glycine
SLC1A4
Glutamate
LAP3
ANPEP
GGT6
OPLAH
GCLM
GCLC
PGD
IDH1
G6PD
NADP+
NADPH
GSR
Glutathione
GPX2
GSSG
NAMPT
Nicotinamide
Nicotinamide-D-ribonucleotide
NMNAT1
NUDT12
NAD+
SLC25A51
NAD+
SIRT4
IDH2
Citrate
Isocitrate
α-Ketoglutarate
SUCLG2
Succinyl CoA
Succinate
Fumarate
Malate
Oxaloacetate
TCA
Acetyl-CoA
CPT2
FASN
MECR
β-oxidation
ROS
ACADVL
HADHB
HADHA
NAD+
NADH
Palmitoyl-carnitine
ACSL1
ACSL3
ACSL4
Palmitic Acid
Palmitoyl-CoA
CPT1C
CPT1A
SPTLC1
3-Dehydro-sphingamine
KDSR
PLPP1
Dihydro-sphingosine-1P
Dihydro-sphingosine
DEGS1
Dihydro-ceramide
Ceramide
ATP6
CV
ATP5PD
CIV
COX7A2
UQCR11
CIII
UQCRB
CYCS
Cytc
ETFDH
ETF:QO
GPD2
mGPDH
CII
CoQ
CI
RET
NDUFA2
NDUFS4
ND5
NDUFA6
NDUFB7
NDUFA7
ND2
e-
ROS
JNK
Bim
NOXA
PUMA
Apoptosis
DHAP
G3P
GDPD1
Lysophosphatidic acid
AGPAT5
MBOAT1
Phosphatidic acid
PLPP1
PLPP3
DGKQ
DGKE
DAG
GPC
PLA2G15
PNPLA6
LPtC
PLA2G4C
PtC
CEPT1
Choline
CHKA
PC
CDP-choline
GPE
LPtE
PtE
Ethanolamine
ETNK1
PE
CDP-ethanolamine
PLD1
PLD3
Digalactosyl-ceramide
GLA
Galactosyl-ceramide
Lactosyl-ceramide
GLB1
Glucosyl-ceramide
GBA2
GBA
Sphingomyelin
SMPD1
Sphingolipid metabolism
mRNA
Protein
mRNA log2(FC)
-2 -1 0 1 2
protein log2(FC)
-1 -0.5 0 0.5 1
Glycerophospholipid metabolism

Figure 3. Lipid and glutamate metabolic alterations converge on ROS generation in TNBC. Overall network model describing metabolic reactions that lead to cancer cell apoptosis after nicotinamide (NAM) treatment. Solid and dotted arrows indicate the direct and indirect reactions, respectively. Color bar indicates the gradient of log2−fold−changes with respect to the comparison of NAM versus control. Unlike the network models in Fig. 1, the node label size was not used to indicate the number of cell types where the corresponding nodes were upregulated because this network shows the changes of both mRNA and protein levels.

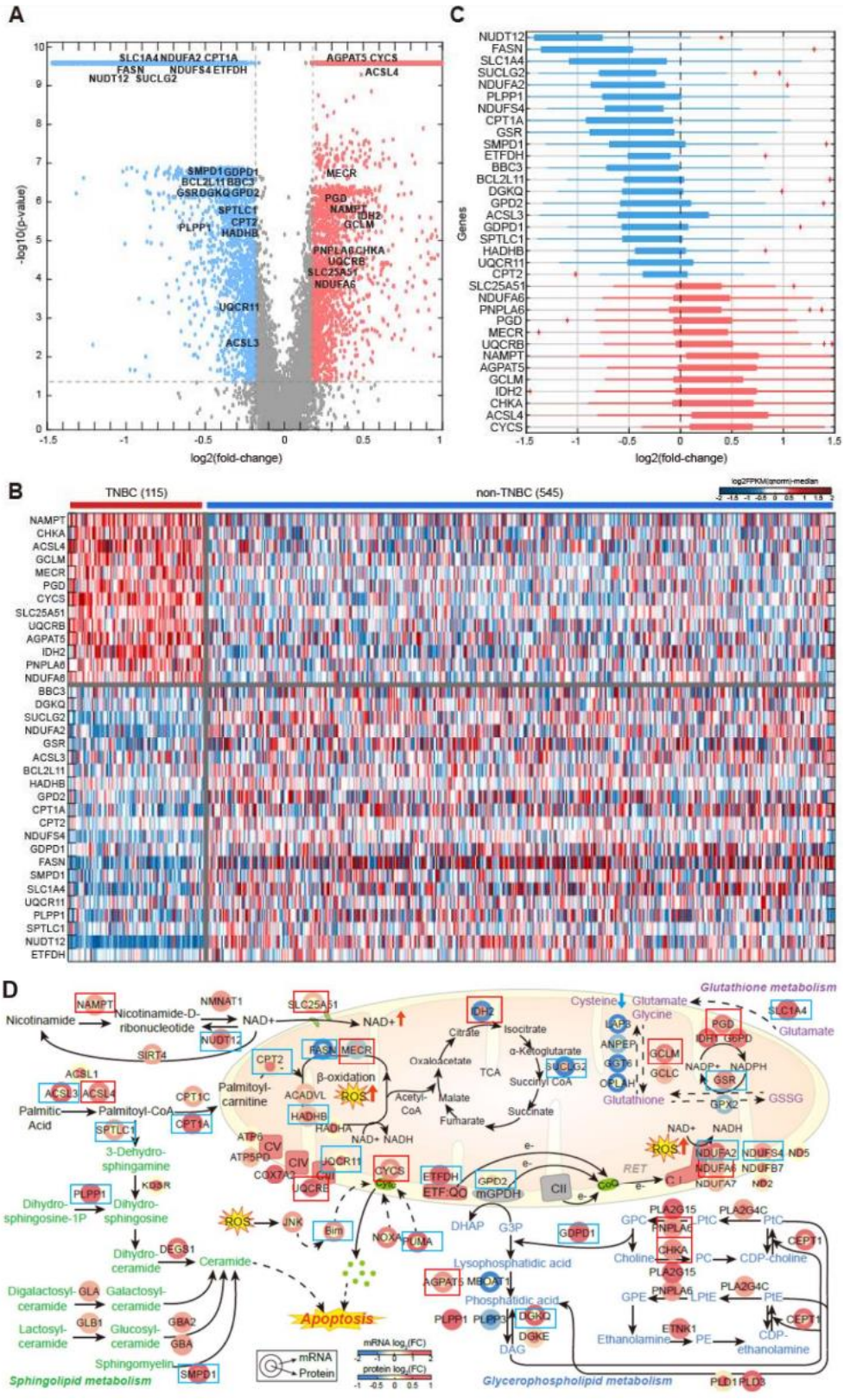
A
SLC1A4 NDUFA2 CPT1A
FASN NDUFS4 ETFDH
NUDT12 SUCLG2
AGPAT5 CYCS
ACSL4
SMPD1 GDPD1
BCL2L11 BBC3
GSRDGKQ GPD2
SPTLC1
CPT2
PLPP1 HADHB
MECR
PGD
NAMPT
IDH2
GCLM
PNPLA6 CHKA
UQCRB
SLC25A51
NDUFA6
UQCR11
ACSL3
-log10(p-value)
log2(fold-change)
C
Genes
log2(fold-change)
B
TNBC (115)
non-TNBC (545)
log2FPKM(norm)-median
D
Glutathione metabolism
Sphingolipid metabolism
Glycerophospholipid metabolism
Apoptosis
mRNA
Protein

Figure S3. Relative mRNA expression levels of key network nodes in TNBC patients with respect to non−TNBC patients in the TCGA breast cancer cohort. (A) Volcano plot for the comparison of TNBC versus non−TNBC (TNBC/non−TNBC). X and Y axes represent log2−fold−changes and the adjusted p−value from the comparison. Dotted lines represent the cutoffs for log2−fold−change and t−test p−value used in this analysis. Pink and blue dots denote the 3,314 upregulated and 3,362 downregulated genes, respectively. The key nodes were indicated in labels. (B) Heat map showing upregulation (red) and downregulation (blue) of 13 and 21 key nodes in TNBC samples, respectively, compared to in non−TNBC samples. The color bar represents the gradient of log2−fold−change of mRNA expression levels. (C) Box plots showing expression changes of 13 upregulated and 21 downregulated key nodes in TNBC samples. Outliers were marked with red crosses. (D) The key nodes in the network model showing upregulation (red box) or downregulation (blue box) in TNBC samples.

3.4. NAM induced mitochondrial dysfunction and ROS-mediated apoptosis in TNBC

To validate suggestions from the transcriptomics and proteomics analyses, we first examined whether NAM influence mitochondrial metabolism and dysregulate mitochondrial activity. We studied the effect of NAM on $\Delta\psi$m (mitochondrial membrane potential), which is associated with the cell's ability to make ATP through OXPHOS [40]. CMXRos staining demonstrated that NAM treatment substantially (BT20, P = 0.009; MDA-MB-468, P = 0.0004; MDA-MB-231, P = 0.002) reduced $\Delta\psi$m in all three TNBC cell types, as seen by flow cytometry (left) and confocal microscopy (right) (Fig. 4A). Staining with JC-1 dye, which accumulates at high $\Delta\psi$m and dissolves at low $\Delta\psi$m [41], indicated that NAM treatment led to mitochondrial depolarization in all TNBC cell types (BT20, P = 0.0043; MDA-MB-468, P = 0.0184; MDA-MB-231, P = 0.0368) (Fig. 4B). To evaluate the dysregulation of ATP synthesis via OXPHOS, we measured the OXPHOS level and real-time ATP production rate in NAM-treated cells using Seahorse XF24 Flux Analyzer. The OCR assay demonstrated that NAM markedly suppressed the mitochondrial OXPHOS process (Fig. 4C), as evidenced by significantly decreased basal respiration (BT20, P = 0.0401; MDA-MB-468, P = 0.0031; MDA-MB-231, P = 0.004), ATP-linked respiration (BT20, P = 0.0296; MDA-MB-468, P = 0.0012; MDA-MB-231, P = 0.0009), maximal respiration (BT20, P = 0.0004; MDA-MB-468, P = 0.0005; MDA-MB-231, P = 0.0008) and proton leak (MDA-MB-468, P = 0.0038) capacity 24 h after NAM treatment (Fig. 4D). These findings revealed that NAM hindered OXPHOS and energy

consumption in TNBC cells via decreasing mitochondrial membrane potential. Thus, according to the above experiments, we could validate that NAM induced mitochondrial damage and dysfunction in TNBC cells.

To establish if NAM triggered ROS-mediated apoptosis in TNBC cells, we treated TNBC cells with dose-escalated NAM (10-100 mm) and then assessed cell viability. The growth of all TNBC cells was decreased in a dose-dependent manner after NAM treatment (Fig. 5A). Flow cytometric analysis also showed that NAM treatment significantly increased the percentage of annexin V-positive apoptotic cells (annexin V+/PI- and annexin V+/PI+ cells) in all TNBC cell types compared with the non-treated control (BT20, 3-61%, $P < 0.0001$; MDA-MB-468, 9-46%, $P < 0.0001$; and MDA-MB-231, 9-34%, $P = 0.0009$) (Fig. 5B). Western blotting of c-PAPR and c-caspase 3 corroborated the increased apoptosis of TNBC cells upon NAM treatment (Fig. 5C). In addition, the pretreatment of TNBC cells with z-VAD.fmk, a pan-caspase inhibitor, significantly suppressed NAM-induced apoptosis (z-VAD/NAM vs NAM, BT20, $P = 0.0011$; MDA-MB-468, $P = 0.0049$; MDA-MB-231, $P = 0.0016$) (Fig. 5D). Collectively, our findings suggested that NAM hindered the growth of TNBC cells by inducing caspase-dependent apoptosis. As deregulated redox metabolism by NAM may play a crucial role in initiating ROS-dependent apoptosis [41], we next investigated whether NAM-induced apoptosis mediated by ROS in TNBC cells. In all the NAM-treated TNBC cell lines, the H2O2 levels were increased by 40-90 times (BT20, $P = 0.0007$; MDA-MB-468, $P = 0.0004$; MDA-MB-231, $P = 0.0028$) (Fig. 5E), and the intracellular ROS levels were increased by double or more in the fluorescence dye DCFH-

DA assay (BT20, P = 0.0227; MDA-MB-468, P = 0.0246; MDA-MB-231, P = 0.0072) (Fig. 5F). In addition, the pretreatment of NAC, an ROS scavenger, followed by the treatment of NAM, showed a significant reduction in NAM-induced cell death in BT20 (P = 0.0044), MDA-MB-468 (P = 0.01) and MDA-MB-231 (P = 0.0012) (Fig. 5G). Therefore, these findings showed that the impact of NAM is mediated by the elevation of intracellular ROS levels, which results in apoptotic cell death in TNBC cells.

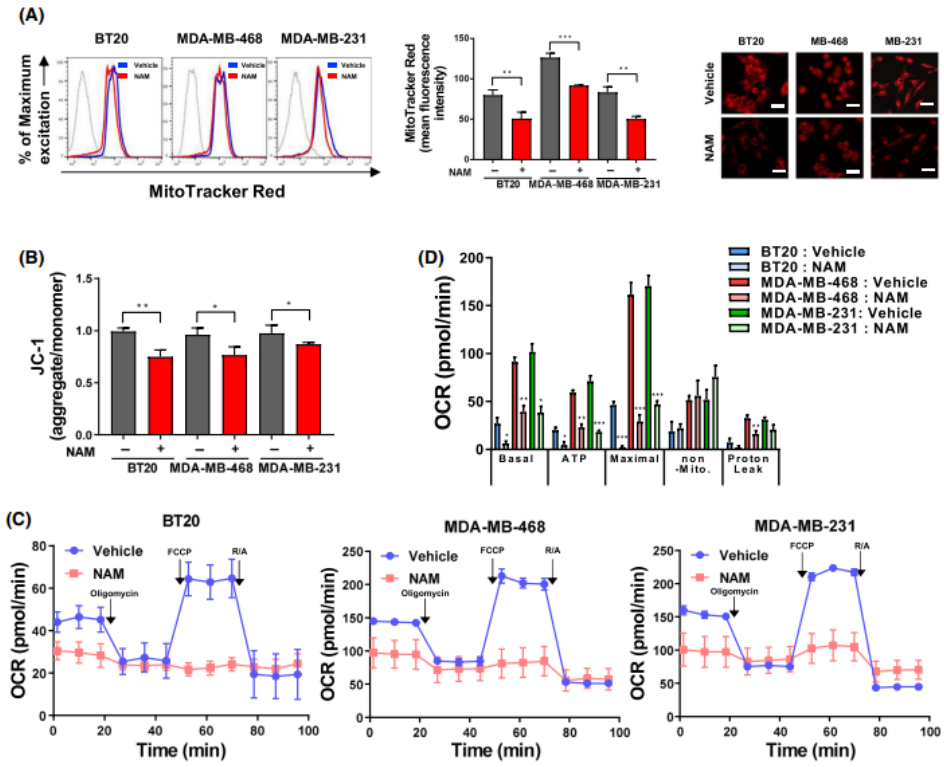

Figure 4. NAM induces mitochondrial dysfunctions in TNBC cells. (A) Mitochondrial membrane potential of triple-negative breast cancer (TNBC) cells after nicotinamide (NAM) treatment (25nM, 24h) was measured using flow cytometry (left) and Mitotracker red staining (250nM) under confocal microscopy (right; scale bar = 100 μm). (B) JC-1 (10nM) fluorescent ratio also suggested that NAM reduced mitochondrial membrane potential. (C) Real-time mitochondrial oxygen consumption rates (OCRs) following NAM treatment were assessed in all TNBC cells by Agilent's Seahorse XF24 analyzer. (D) Representative graphs illustrating the quantification of the basal-, ATP-linked-, maximal-, nonmitochondrial-OCR and proton leak after NAM treatment.

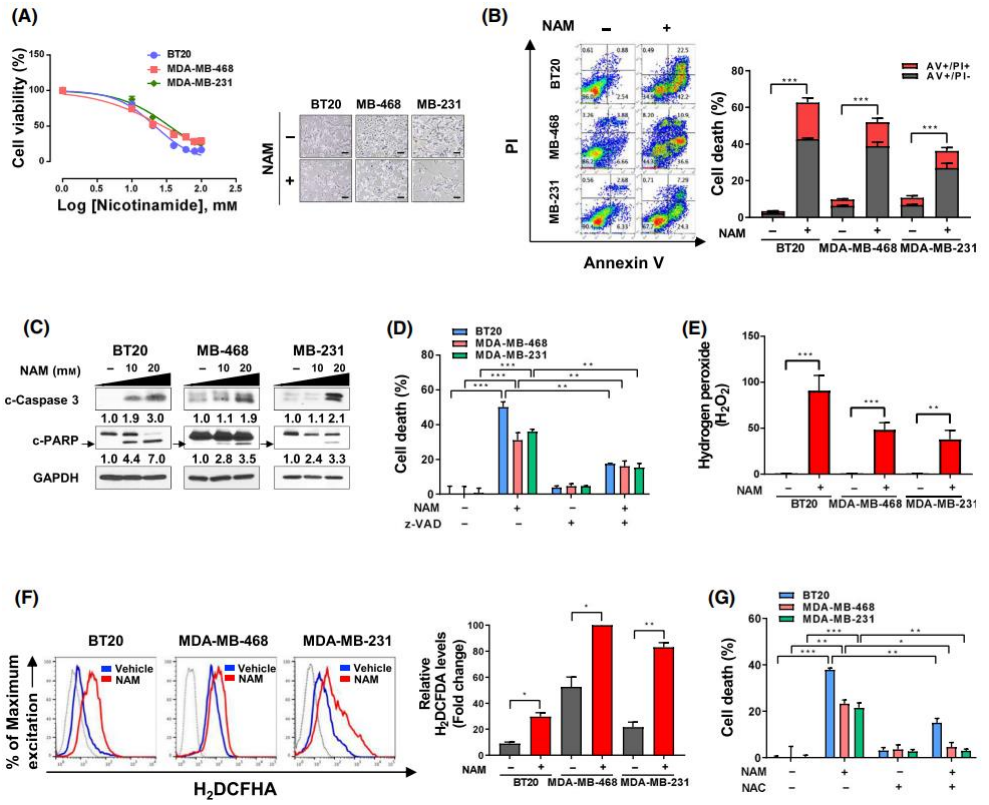

Figure 5. NAM induces ROS-mediated apoptosis in TNBC cells. (A) Triple-negative breast cancer (TNBC) cells were treated with increasing concentrations (10-100 mM) of nicotinamide (NAM) for 48 h (left), and cell viability was determined by CellTiter-Glo Luminescent Cell Viability assay. Representative phase-contrast images after NAM treatment (right; scale bar = 100 μm). (B) Flow cytometry images of TNBC cells (left) after 48 h of NAM treatment (BT20, 20 mM; MDA-MB-468 and MDA-MB-231, 40 mM). Apoptosis was determined by Annexin V (AV)/PI-staining (AV+/PI and AV+/PI+ cell distribution). The percentage (%) of apoptotic TNBC cells (right) after NAM treatment. (C) Measurement of c-caspase 3 and c-poly (ADP-ribose) polymerase (c-PARP) (arrow) expression by western blot after NAM treatment for 48 h in TNBC cells. GAPDH served as a loading control. Western blot bands were

quantified by densitometry using the IMAGEJ software. (D) The cytotoxicity effect of NAM treatment was measured, with or without z-VAD.fmk pre-treatment (10 μM; 1 h). Cell death was accessed using CellTiter-Glo Luminescent Cell Viability assay. (E) Cytoplasmic hydrogen peroxide (H2O2) was measured by ROS-Glo H2O2 assay in the presence or absence of NAM (25 mM). (F) Intracellular reactive oxygen species (ROS) after NAM treatment was assessed using a DCFH-DA staining (5 μM) by flow cytometry (left) and mean fluorescence intensity (MFI) analysis (right). (G) NAM-induced cell death altered by 1 mM of N-acetyl-L-cysteine (NAC) pre-treatment for 2 h. Bar graphs are presented in mean ± SEM from triplicate experiment (a two-tailed t-test, *P < 0.05, **P < 0.01, ***P < 0.001). (Abbreviations: z-VAD, carbobenzoxy-valyl-alanyl-aspartyl-[O-methyl]-fluoromethylketone).

Chapter 4. Discussion

Metabolic reprogramming by transforming and building biomass is a general characteristic of tumors to obtain energy so that tumor cells can sustain proliferation and survival in a nutrient-deprived environment [42,43]. TNBC is characterized by its dependence on non-canonical de-novo fatty acid synthesis to fulfil the excessive energy requirement [44]. In a previous xenograft experiment, the inhibition of fatty acid synthase in combination with an anti-EGFR agent showed synergetic effects against TNBC [45]. The replenishment of NAM has been recently suggested as a new modulator of lipid metabolism in animal models [46]. These findings provided a new strategy for modulating lipid metabolism for TNBC treatment.

In this study, we showed NAM-induced metabolic disruption in TNBC and the potential role of NAM supplementation as a novel therapeutic agent for TNBC using the analysis of multi-omics systems biology. In our network modelling analysis, the perturbation of lipid metabolism was prominent after NAM treatment. Interestingly, the altered lipogenic pathways including fatty acid β-oxidation and glycerophospholipid and sphingolipid metabolism converged into apoptosis in TNBC by facilitating ROS generation. Significant upregulation of fatty acid β-oxidation was observed after NAM treatment, which is concordant with a previous report wherein the over-reduction of OXPHOS CI and coenzyme Q pool by fatty acid β-oxidation could shuttle electron sources to RET and stimulate RET-ROS production [35]. In the glycerophospholipid catabolic pathway, GDPD1 and GPD2 (mitochondrial glycerol 3-phosphate dehydrogenase) were significantly upregulated in NAM-treated

TNBC cells. The reduction of G3P by GPD2 was previously shown to mediate RET and overproduce RET-ROS in mitochondrial OXPHOS CI much faster than pyruvate- or malate-dependent ROS production [47]. Along with the glycerophospholipid pathway, SPTLC1, ATF6 and SMPD1, the key genes associated with the sphingolipid pathway, were also upregulated by NAM treatment. In this cascade, SMPD1 upregulation was expected to build up ceramide, which induces ROS generation, lysosomal degradation and cell death [48,49]. In addition to the support of these lipogenic disturbances, we found that NAM-induced RET-ROS accumulation was dependent on dysregulated OXPHOS and NAD+/NADH imbalance. Based on these findings, we proposed RET-induced ROS as a therapeutic mechanism of NAM in TNBC; that is, NAM-mediated RET-ROS induces mitochondria-dependent apoptosis. ROS are important signaling molecules involved in energy metabolic processes and play key roles in redox homeostasis in cancer [50,51]. Recently, alterations in ROS-related molecular processes have emerged as the hallmarks of TNBC and provided a basis for targeting ROS-induced metabolic disruption for TNBC treatment [40,52,53]. A reverse flow of electron in mitochondrial CI constitutes a considerable source of ROS production, i.e. RET-induced ROS, which has been implicated in physiologic conditions, including myoblast differentiation, macrophage immune reaction, oxygen sensing in the carotid body and longevity and in pathologic processes, including ischemia-reperfusion injury [34]. In cancer, the role of RET-induced ROS is still unclear [34,52]. The tumor microenvironment involves recurrent oxidative stress or ischemic injury, and the RET process might take place in the environment for the control of ROS homeostasis [52]. In addition, there has been other evidence suggesting constitutive promotion of

RET in mitochondria, instead of canonical ATP synthesis, in TNBC cells [52,54]. Thus, our data indicate a pioneering approach using RET-ROS in TNBC treatment.

We focused on cellular pathways upregulated by NAM. However, NAM downregulated cell proliferation, adhesion and migration, as well as immune response. Cell proliferation and adhesion/migration are expected to be decreased given the increased ROS. However, how the decrease of the immune-related genes/proteins measured from TNBC cells may affect their associated tumor microenvironment is not clear. To explore this aspect. we reconstructed a network model describing interactions among the downregulated genes involved in the immune-related processes (inflammatory response, TLR/NF-kB/MAPK signaling, cytokine production, and response to cytokine in Figs 2E and 3G) in NAM-treated TNBC cells (Fig. S4). The network seems to indicate that the increased ROS from RET and lipid metabolism (Fig. 4) inactivates PI3K/AKT signaling for survival of TNBC cells. This may result in an initial decrease in cytokine production, which then lessens activation of JAK/STAT and MAPK signaling in TNBC cells. As a result of the collective actions of these decreased signaling pathways, the final decreased cytokine milieu appears to be determined. These decreased cytokines include IL1 β and LTB, which reduce the activation of MYD88/TRAF2 signaling and in turn the activation of NF-kB signaling together with the decreased CD14 (TLR4 co-receptor). Interestingly, these cytokines act on tumor-associated macrophage (TAM, CCL2/5 and CSF1), myeloid-derived suppressive cell (MDSC, CCL2/5 and CXCL1/2/5/8/10) and regulatory T-cell (Treg, CCL2/5/22 and CXCL10) (Fig. S4, table), which are known to suppress the activation of cytotoxic T-cells, a central player in anti-tumor immunity. The decrease of these

cytokines suggest that NAM might increase the activation of cytotoxic T-cells and thus promote an immune surveillance environment.

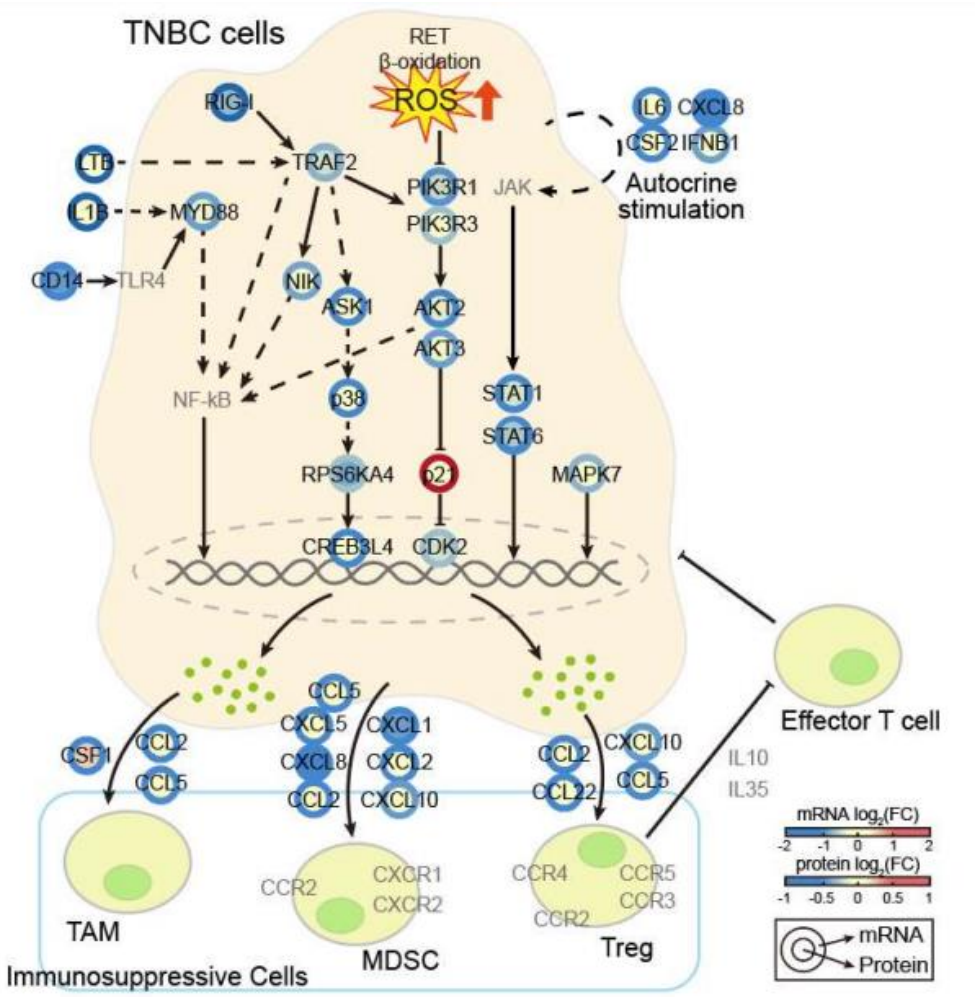

Cytokines	Targets	References
CCL2	MDSC	Kumar V., et al. (2016). Trends in immunology, 37(3), 208–220.
	TAM	Hao, Q., et al. (2020). Cell communication and signaling : CCS, 18(1), 82.
	Treg	Chang, A. L., et al. (2016). Cancer research, 76(19), 5671–5682.
CCL5	MDSC	Kumar V., et al. (2016). Trends in immunology, 37(3), 208–220.
	TAM	Gao, D., et al. (2017) BMC cancer, 17(1), 834.
	Treg	Tan, M. C., et al. (2009). Journal of immunology (Baltimore, Md. : 1950), 182(3), 1746–1755

CCL22	Treg	Gobert, M., et al. (2009). Cancer research, 69(5), 2000–2009
CSF1	TAM	Ding, J., et al. (2016). International journal of oncology, 49(5), 2064–2074.
CSF2	Autocrine	Bhattacharya, P., et al. (2015). Cytokine, 75(2), 261–271.
CXCL1	MDSC	Shi, H., et al. (2018). Cancer science, 109(12), 3826–3839.
CXCL2	MDSC	Shi, H., et al. (2018). Cancer science, 109(12), 3826–3839.
CXCL5	MDSC	Zhang, W., et al. (2020). Cancer communications (London, England), 40(2-3), 69–80.
CXCL8	MDSC	Alfaro, C., et al. (2016). Clinical cancer research : an official journal of the American Association for Cancer Research, 22(15), 3924–3936
	Autocrine	Campbell, L. M., et al. (2013). Pharmaceuticals (Basel, Switzerland), 6(8), 929–959.
CXCL10	MDSC	Liu, H., et al. (2021). Cell death & disease, 12(5), 489.
	Treg	Li, C. X., et al. (2016). Journal of hepatology, 65(5), 944–952.
IFNB1	Autocrine	Yarilina, A., et al. (2008). Nature immunology, 9(4), 378–387.
IL6	Autocrine	Grivennikov, S., et al. (2008). Cancer cell, 13(1), 7–9.
IL1B	NF-kB signaling	Kawai, T., et al. (2007). Trends in molecular medicine, 13(11), 460–469.
LTB	NF-kB signaling	Chang, Y. H., et al. (2002). Experimental cell research, 278(2), 166–174..

Figure S4. A network model for the decreased immune response in NAM-treated TNBC cells. Arrows indicate directions of the reactions, and dotted arrows indicate indirect reactions involving intermediate reactions between the nodes. Node colors represent up (red) and downregulation (blue) of the corresponding genes (node boundary) or proteins (node center). Color bar, gradient of log2-fold-changes in NAM versus control. The maximum of absolute log2-fold-changes in the three cell types were chosen for the node

colors. Node label size denotes whether the corresponding gene was identified as a DEG in three (large), two (middle), or one (small) of the cell types. Grey node labels denote that the corresponding nodes are non-DEGs in the three cell types. Previous studies reporting actions of cytokines on their target cells indicated in the network model are summarized in the table.

Chapter 5. Conclusion

In conclusion, our findings revealed a conceptual signaling mechanism in which NAM induces bifurcating metabolic changes (RET and lipogenic pathways) in TNBC and enhances the ROS-induced apoptotic pathway. These findings suggest NAM's potential as a metabolic antitumor medication that targets TNBC as well as other types of tumor. Future research should involve clinical trials of NAM including TNBC patients in order to assess the effectiveness of NAM supplementation and optimize the dosage of NAM in a therapeutic context.

Bibliography

1. Gupta, G.K., Collier, A.L., Lee, D., Hoefer, R.A., Zheleva, V., Siewertsz van Reesema, L.L., Tang-Tan, A.M., Guye, M.L., Chang, D.Z., Winston, J.S., *et al.* (2020). Perspectives on Triple-Negative Breast Cancer: Current Treatment Strategies, Unmet Needs, and Potential Targets for Future Therapies. Cancers (Basel) *12*.
2. Foulkes, W.D., Smith, I.E., and Reis, J.S. (2010). Triple-Negative Breast Cancer. New Engl J Med *363*, 1938-1948.
3. Yin, L., Duan, J.J., Bian, X.W., and Yu, S.C. (2020). Triple-negative breast cancer molecular subtyping and treatment progress. Breast Cancer Res *22*, 61.
4. Cocco, S., Piezzo, M., Calabrese, A., Cianniello, D., Caputo, R., Lauro, V.D., Fusco, G., Gioia, G.D., Licenziato, M., and De Laurentiis, M. (2020). Biomarkers in Triple-Negative Breast Cancer: State-of-the-Art and Future Perspectives. Int J Mol Sci *21*.
5. Hanahan, D., and Weinberg, R.A. (2011). Hallmarks of cancer: the next generation. Cell *144*, 646-674.
6. Luengo, A., Gui, D.Y., and Vander Heiden, M.G. (2017). Targeting Metabolism for Cancer Therapy. Cell Chem Biol *24*, 1161-1180.
7. De, A., and Kuppusamy, G. (2020). Metformin in breast cancer: preclinical and clinical evidence. Curr Probl Cancer *44*, 100488.
8. Goard, C.A., Chan-Seng-Yue, M., Mullen, P.J., Quiroga, A.D., Wasylishen, A.R., Clendening, J.W., Sendorek, D.H., Haider, S., Lehner, R., Boutros, P.C., *et al.* (2014). Identifying molecular features that distinguish fluvastatin-sensitive breast tumor cells. Breast Cancer Res Treat *143*, 301-312.
9. Maiese, K., Chong, Z.Z., Hou, J., and Shang, Y.C. (2009). The vitamin nicotinamide: translating nutrition into clinical care. Molecules *14*, 3446-3485.
10. Santidrian, A.F., Matsuno-Yagi, A., Ritland, M., Seo, B.B., LeBoeuf, S.E., Gay, L.J., Yagi, T., and Felding-Habermann, B. (2013). Mitochondrial complex I activity and NAD+/NADH balance regulate breast cancer progression. J Clin Invest *123*, 1068-1081.
11. Audrito, V., Vaisitti, T., Rossi, D., Gottardi, D., D'Arena, G., Laurenti, L., Gaidano, G., Malavasi, F., and Deaglio, S. (2011). Nicotinamide blocks proliferation and induces apoptosis of chronic lymphocytic leukemia cells through activation of the p53/miR-34a/SIRT1 tumor suppressor network. Cancer Res *71*, 4473-4483.

12. Kim, W.J., Lee, J.W., Quan, C., Youn, H.J., Kim, H.M., and Bae, S.C. (2011). Nicotinamide inhibits growth of carcinogen induced mouse bladder tumor and human bladder tumor xenograft through up-regulation of RUNX3 and p300. J Urol *185*, 2366-2375.
13. Dominguez-Gomez, G., Diaz-Chavez, J., Chavez-Blanco, A., Gonzalez-Fierro, A., Jimenez-Salazar, J.E., Damian-Matsumura, P., Gomez-Quiroz, L.E., and Duenas-Gonzalez, A. (2015). Nicotinamide sensitizes human breast cancer cells to the cytotoxic effects of radiation and cisplatin. Oncol Rep *33*, 721-728.
14. Kim, J.Y., Lee, H., Woo, J., Yue, W., Kim, K., Choi, S., Jang, J.J., Kim, Y., Park, I.A., Han, D.*, et al.* (2017). Reconstruction of pathway modification induced by nicotinamide using multi-omic network analyses in triple negative breast cancer. Sci Rep *7*, 3466.
15. Martin, M. (2011). Cutadapt removes adapter sequences from high-throughput sequencing reads. 2011 *17*, 3.
16. Trapnell, C., Pachter, L., and Salzberg, S.L. (2009). TopHat: discovering splice junctions with RNA-Seq. Bioinformatics *25*, 1105-1111.
17. Anders, S., Pyl, P.T., and Huber, W. (2015). HTSeq--a Python framework to work with high-throughput sequencing data. Bioinformatics *31*, 166-169.
18. Trapnell, C., Williams, B.A., Pertea, G., Mortazavi, A., Kwan, G., van Baren, M.J., Salzberg, S.L., Wold, B.J., and Pachter, L. (2010). Transcript assembly and quantification by RNA-Seq reveals unannotated transcripts and isoform switching during cell differentiation. Nat Biotechnol *28*, 511-515.
19. Chae, S., Ahn, B.Y., Byun, K., Cho, Y.M., Yu, M.H., Lee, B., Hwang, D., and Park, K.S. (2013). A systems approach for decoding mitochondrial retrograde signaling pathways. Sci Signal *6*, rs4.
20. Bolstad, B.M., Irizarry, R.A., Astrand, M., and Speed, T.P. (2003). A comparison of normalization methods for high density oligonucleotide array data based on variance and bias. Bioinformatics *19*, 185-193.
21. Wisniewski, J.R., Zougman, A., Nagaraj, N., and Mann, M. (2009). Universal sample preparation method for proteome analysis. Nat Methods *6*, 359-362.
22. Han, D., Moon, S., Kim, Y., Kim, J., Jin, J., and Kim, Y. (2013). In-depth proteomic analysis of mouse microglia using a combination of FASP and StageTip-based, high pH, reversed-phase fractionation. PROTEOMICS *13*, 2984-2988.
23. Huang, D.W., Sherman, B.T., and Lempicki, R.A. (2009). Systematic and integrative analysis of large gene lists using DAVID bioinformatics resources. Nature Protocols *4*, 44-57.

24. Dice, L.R. (1945). Measures of the Amount of Ecologic Association Between Species. Ecology *26*, 297-302.
25. Mueller, L.N., Rinner, O., Schmidt, A., Letarte, S., Bodenmiller, B., Brusniak, M.Y., Vitek, O., Aebersold, R., and Müller, M. (2007). SuperHirn - a novel tool for high resolution LC-MS-based peptide/protein profiling. Proteomics *7*, 3470-3480.
26. Shannon, P., Markiel, A., Ozier, O., Baliga, N.S., Wang, J.T., Ramage, D., Amin, N., Schwikowski, B., and Ideker, T. (2003). Cytoscape: a software environment for integrated models of biomolecular interaction networks. Genome Res *13*, 2498-2504.
27. Morris, J.H., Apeltsin, L., Newman, A.M., Baumbach, J., Wittkop, T., Su, G., Bader, G.D., and Ferrin, T.E. (2011). clusterMaker: a multi-algorithm clustering plugin for Cytoscape. BMC Bioinformatics *12*, 436.
28. Kanehisa, M., and Goto, S. (2000). KEGG: kyoto encyclopedia of genes and genomes. Nucleic Acids Res *28*, 27-30.
29. Kanehisa, M. (2019). Toward understanding the origin and evolution of cellular organisms. Protein Sci *28*, 1947-1951.
30. Kanehisa, M., Furumichi, M., Sato, Y., Ishiguro-Watanabe, M., and Tanabe, M. (2021). KEGG: integrating viruses and cellular organisms. Nucleic Acids Res *49*, D545-D551.
31. Grossman, R.L., Heath, A.P., Ferretti, V., Varmus, H.E., Lowy, D.R., Kibbe, W.A., and Staudt, L.M. (2016). Toward a Shared Vision for Cancer Genomic Data. N Engl J Med *375*, 1109-1112.
32. Lee, K.M., Hwang, E.H., Kang, S.E., Lee, C.H., Lee, H., Oh, H.J., Kim, K., Koh, J., and Ryu, H.S. (2020). Tryptophanyl-tRNA Synthetase Sensitizes Hormone Receptor-Positive Breast Cancer to Docetaxel-Based Chemotherapy. J Breast Cancer *23*, 599-609.
33. Luongo, T.S., Eller, J.M., Lu, M.J., Niere, M., Raith, F., Perry, C., Bornstein, M.R., Oliphint, P., Wang, L., McReynolds, M.R., *et al.* (2020). SLC25A51 is a mammalian mitochondrial NAD(+) transporter. Nature *588*, 174-179.
34. Scialo, F., Fernandez-Ayala, D.J., and Sanz, A. (2017). Role of Mitochondrial Reverse Electron Transport in ROS Signaling: Potential Roles in Health and Disease. Front Physiol *8*, 428.
35. Guaras, A., Perales-Clemente, E., Calvo, E., Acin-Perez, R., Loureiro-Lopez, M., Pujol, C., Martinez-Carrascoso, I., Nunez, E., Garcia-Marques, F., Rodriguez-Hernandez, M.A., *et al.* (2016). The CoQH2/CoQ Ratio Serves as a Sensor of Respiratory Chain Efficiency. Cell Rep *15*, 197-209.
36. Bowlby, S.C., Thomas, M.J., D'Agostino, R.B., Jr., and Kridel, S.J. (2012). Nicotinamide phosphoribosyl transferase (Nampt) is required for de novo lipogenesis in tumor cells. PLoS One *7*, e40195.

37. Pettus, B.J., Chalfant, C.E., and Hannun, Y.A. (2002). Ceramide in apoptosis: an overview and current perspectives. Biochim Biophys Acta *1585*, 114-125.
38. Verheij, M., Bose, R., Lin, X.H., Yao, B., Jarvis, W.D., Grant, S., Birrer, M.J., Szabo, E., Zon, L.I., Kyriakis, J.M., *et al.* (1996). Requirement for ceramide-initiated SAPK/JNK signalling in stress-induced apoptosis. Nature *380*, 75-79.
39. Mracek, T., Drahota, Z., and Houstek, J. (2013). The function and the role of the mitochondrial glycerol-3-phosphate dehydrogenase in mammalian tissues. Biochim Biophys Acta *1827*, 401-410.
40. Ciccarese, F., and Ciminale, V. (2017). Escaping Death: Mitochondrial Redox Homeostasis in Cancer Cells. Front Oncol *7*, 117.
41. Feng, Y., Wang, Y., Jiang, C., Fang, Z., Zhang, Z., Lin, X., Sun, L., and Jiang, W. (2017). Nicotinamide induces mitochondrial-mediated apoptosis through oxidative stress in human cervical cancer HeLa cells. Life Sci *181*, 62-69.
42. DeBerardinis, R.J., and Chandel, N.S. (2016). Fundamentals of cancer metabolism. Sci Adv *2*, e1600200.
43. Pavlova, N.N., and Thompson, C.B. (2016). The Emerging Hallmarks of Cancer Metabolism. Cell Metab *23*, 27-47.
44. Menendez, J.A., and Lupu, R. (2007). Fatty acid synthase and the lipogenic phenotype in cancer pathogenesis. Nat Rev Cancer *7*, 763-777.
45. Giro-Perafita, A., Palomeras, S., Lum, D.H., Blancafort, A., Vinas, G., Oliveras, G., Perez-Bueno, F., Sarrats, A., Welm, A.L., and Puig, T. (2016). Preclinical Evaluation of Fatty Acid Synthase and EGFR Inhibition in Triple-Negative Breast Cancer. Clin Cancer Res *22*, 4687-4697.
46. Yu, X., Xue, M., Liu, Y., Zhou, Z., Jiang, Y., Sun, T., and Liang, H. (2021). Effect of nicotinamide riboside on lipid metabolism and gut microflora-bile acid axis in alcohol-exposed mice. Food Sci Nutr *9*, 429-440.
47. Mracek, T., Pecinova, A., Vrbacky, M., Drahota, Z., and Houstek, J. (2009). High efficiency of ROS production by glycerophosphate dehydrogenase in mammalian mitochondria. Arch Biochem Biophys *481*, 30-36.
48. Ogretmen, B., and Hannun, Y.A. (2004). Biologically active sphingolipids in cancer pathogenesis and treatment. Nat Rev Cancer *4*, 604-616.
49. Park, W.J., and Park, J.W. (2020). The role of sphingolipids in endoplasmic reticulum stress. FEBS Lett *594*, 3632-3651.
50. Chandel, N.S. (2015). Evolution of Mitochondria as Signaling

Organelles. Cell Metab *22*, 204-206.
51. Sena, L.A., and Chandel, N.S. (2012). Physiological roles of mitochondrial reactive oxygen species. Mol Cell *48*, 158-167.
52. Raimondi, V., Ciccarese, F., and Ciminale, V. (2020). Oncogenic pathways and the electron transport chain: a dangeROS liaison. Br J Cancer *122*, 168-181.
53. Sun, X., Wang, M., Wang, M., Yu, X., Guo, J., Sun, T., Li, X., Yao, L., Dong, H., and Xu, Y. (2020). Metabolic Reprogramming in Triple-Negative Breast Cancer. Front Oncol *10*, 428.
54. Sanchez-Arago, M., Formentini, L., Martinez-Reyes, I., Garcia-Bermudez, J., Santacatterina, F., Sanchez-Cenizo, L., Willers, I.M., Aldea, M., Najera, L., Juarranz, A.*, et al.* (2013). Expression, regulation and clinical relevance of the ATPase inhibitory factor 1 in human cancers. Oncogenesis *2*, e46.

Abstract in Korean

삼중음성유방암에 대한 니코틴아마이드의 항암 대사 기작에 관한 오믹스 연구

삼중음성유방암(triple-negative breast cancer, TNBC)은 유방암의 분자학적 아형 중 가장 공격적이고 예후가 좋지 않은 아형이다. 그러나 TNBC는 타켓팅 할 수 있는 단백질이 없기 때문에 표적 치료법과 같은 방법을 사용할 수 없어 치료가 어렵다. 따라서 삼중음성유방암에 대한 새로운 치료 접근법이 필요하다. 니코틴아마이드(nicotinamide, NAM)는 미토콘드리아 대사 및 산화환원 반응에 중요한 역할을 하는 니아신(비타민 B3)의 수용성 아미드 유도체이다. 기존 연구에 의하면, 니코틴아마이드가 삼중음성유방암을 포함한 다양한 암세포의 성장과 진행을 억제하는 것으로 나타났다. 이 논문에서 우리는 니코틴아마이드 처리시 조절되는 세포의 대사과정과 삼중음성유방암에 대한 니코틴아마이드의 항암 효과 사이의 구체적인 연관성을 밝히기 위해 멀티오믹스 분석 접근법을 적용했다. 니코틴아마이드는 미토콘드리아 막 전위 및 아데노신삼인산 (ATP) 생성을 감소시키고, 삼중음성유방암에서 역전자전달(reverse electron transport, RET), 지방산 산화, 글리세로인지질/스핑고지질 대사 과정을 증가시켜 활성산소종(reactive oxygen species, ROS)을 증가시켰다. 높은 수준의 활성산소종은 세포사멸을 유도하고 암세포 발달을 억제한다고 알려져 있다. 이 논문에서는 니코틴아마이드가 삼중음성유방암에서 미토콘드리아 오작동을 통한 암세포 사멸을 유발하고, 크게 두가지 갈래의 물질대사(RET 및 지질 대사)를 조절하여 과도한 활성산소종 생성을 유발한다는 것을 밝혀냈다. 우리는 니코틴아마이드가 삼중음성유방암 치료를 위한 차세대 항암제로서의 잠재력이 있음을 제안하며, 나아가 이 연구가 니코틴아마이드가 임상연구에 보다 적극적으로 활용되는

기반을 마련할 것임을 기대한다.

주요어 : 삼중음성유방암, 니코틴아마이드, 기능유전체학, 암 대사과정, 활성산소종
학 번 : 2020-21313